2019

Major shifts in nutrient and phytoplankton dynamics in the North Pacific Subtropical Gyre over the last 5000 years revealed by high-resolution proteinaceous deep-sea coral $\delta^{15}N$ and $\delta^{13}C$ records

Danielle S. Glynn

Kelton W. McMahon

See next page for additional authors

Authors
Danielle S. Glynn, Kelton W. McMahon, Thomas P. Guilderson, and Matthew D. McCarthy

Major shifts in nutrient and phytoplankton dynamics in the North Pacific Subtropical Gyre over the last 5000 years revealed by high-resolution proteinaceous deep-sea coral $\delta^{15}N$ and $\delta^{13}C$ records

Danielle S. Glynn[1*], Kelton W. McMahon[1,2], Thomas P. Guilderson[1,3], Matthew D. McCarthy[1]

1. Ocean Sciences Department, University of California, Santa Cruz, Santa Cruz, CA 95064 USA
2. Graduate School of Oceanography, University of Rhode Island, Narragansett, RI 02882 USA
3. Center for Accelerator Mass Spectrometry, Lawrence Livermore National Laboratory, Livermore, CA 94550 USA
* Corresponding Author: dglynn@ucsc.edu

Abstract

The North Pacific Subtropical Gyre (NPSG) is the largest continuous ecosystem on Earth and is a critical component of global oceanic biogeochemical cycling and carbon sequestration. We report here multi-millennial-scale, sub-decadal-resolution records of bulk stable nitrogen ($\delta^{15}N$) and carbon ($\delta^{13}C$) isotope records from proteinaceous deep-sea corals. Data from three *Kulamanamana haumeaae* specimens from the main Hawaiian Islands extend coral-based time-series back ~5000 years for the NPSG and bypass constraints of low resolution sediment cores in this oligotrophic ocean region. We interpret these records in terms of shifting biogeochemical cycles and plankton community structure, with a main goal of placing the extraordinarily rapid ecosystem biogeochemical changes documented by recent coral records during the Anthropocene in a context of broader Late-Holocene variability.

During intervals where new data overlaps with previous records, there is strong correspondence in isotope values, indicating that this older data represents a direct extension of Anthropocene records. These results reveal multiple large isotopic shifts in both $\delta^{15}N$ and $\delta^{13}C$ values similar in magnitude to those reported in last 150 years (~1.5‰ for $\delta^{15}N$ and ~1.2 ‰ for Seuss-corrected $\delta^{13}C$). This shows that large fluctuations in isotope value of export production in this region are not unique to the recent past, but have occurred multiple times through the Mid- to Late-Holocene. However, these earlier isotopic shifts occurred over much longer time intervals (~millennial vs. decadal time scales). Further, the $\delta^{15}N$ data confirm that the extremely low present day $\delta^{15}N$ values recorded by deep sea corals (~8‰) are unprecedented for the NPSG, at least within the past five millennia.

Together these records reveal centennial to millennial-scale oscillations in NPSG biogeochemical cycles. Further, these data also suggest a number of independent biogeochemical

regimes during which $\delta^{15}N$ and $\delta^{13}C$ trends were synchronous (similar to recent coral records) or distinctly decoupled. We propose that phytoplankton species composition and nutrient source changes are the dominant mechanisms controlling the coupling and de-coupling of $\delta^{15}N$ and $\delta^{13}C$ values, likely primarily influenced by changing oceanographic conditions (e.g., stratification vs. entrainment). The decoupling observed in the past further suggests that oceanographic forcing and ecosystem responses controlling $\delta^{15}N$ and $\delta^{13}C$ values of export production have been substantially different earlier in the Holocene compared to mechanisms controlling the present day system.

Key Words: carbon; nitrogen; isotopes; paleoclimate; Holocene; deep-sea coral; North Pacific Subtropical Gyre; phytoplankton; biogeochemical cycling

1. Introduction

Modern subtropical gyres are characterized by low nutrient concentrations and low primary production, with biogeochemical cycles typically dominated by microbial loop dynamics (Karl, 1999). These oligotrophic gyre systems comprise around 60% of the global oceans and are critical components of the global marine biogeochemical balance (Karl, 1999). It is now recognized that aggregate open-ocean oligotrophic regions, due to their vast extent, contribute the bulk of marine productivity and account for a substantial amount of global ocean export (Karl et al., 1997; Martin et al., 1987).

The North Pacific Subtropical Gyre (NPSG) is the largest contiguous ecosystem on earth, and remote sensing indicates that it is rapidly expanding (Polovina et al., 2008). In contrast to global trends of declining marine productivity, phytoplankton communities of the NPSG are increasing in both biomass and productivity (Boyce et al., 2010; Corno et al., 2007; Karl et al., 2001). This is due to changes in plankton community structure, which appear to be linked to the addition of new nutrient sources from expanding communities of nitrogen-fixing diazotrophs, selected for by increased stratification (Karl et al., 1997; Karl et al., 2001; Karl et al., 2011). As such, understanding how algal community structure and nutrient supply have responded to physical forcing in the past is critical to understanding future changes in the ecosystem dynamics of these critical open ocean systems. As part of the Hawaiian Ocean Time-Series (HOT) program, instrumental observations taken at station ALOHA (22°45’W, 158°W) suggest that variability in physical and biological attributes of the NPSG are coupled to inter-annual climate variability superimposed upon longer term, basin-wide variability (Corno et al., 2007; Di Lorenzo et al., 2008). While much can be gained from detailed instrumental records at ALOHA

and other time-series stations, the short time scale of these records is inadequate to understand the coupling of biogeochemical cycles to long term climate forcing. Further, the low sedimentation rate in oligotrophic regions, such as the NPSG, means the entire Holocene is recorded in ~10 cm of bioturbated sediments, leading at best to uncertain, low resolution sediment records.

Cosmopolitan deep-sea proteinaceous corals are unique biogenic archives that can provide centennial to millennial-scale records at sub-decadal resolution of past ocean conditions. These azooxanthellate corals are low-order consumers which feed on recently exported particulate organic matter (POM), and record the isotopic signatures of this food source into the accretionary growth layers of proteinaceous skeletons (Roark et al., 2009; Sherwood et al., 2014; McMahon et al., 2017). The horny proteinaceous skeleton is composed of a fibrillar protein framework (Ehrlich et al., 2006) that is resistant to degradation (Sherwood et al., 2006). The Hawaiian gold coral *Kulamanamana haumeaae*, a colonial zoanthid, is extraordinarily long-lived, thus providing a bioarchive on multi-millennial time scales for the NPSG region with average radial growth rates in the low tens of microns per year (Guilderson et al., 2013; Roark et al., 2009).

Previous records from the NPSG Hawaiian Islands spanning the last ~1000 years have shown dramatic decreases in both nitrogen ($\delta^{15}N$; Sherwood et al. 2014) and carbon ($\delta^{13}C$; McMahon et al. 2015) isotopic values since the Little Ice Age (~1850 CE). These data indicate that both $\delta^{15}N$ and $\delta^{13}C$ values of exported primary production have strongly decreased, commensurate with 20th century warming and gyre expansion. Sherwood et al. (2014) used a

multi-proxy compound-specific stable isotope approach to show that the declining deep-sea coral $\delta^{15}N$ values were indicative of an increase in the relative contribution of nitrogen fixation supporting export production in the NPSG over the last 150 yrs. McMahon et al. (2015) then used a compound-specific stable isotope fingerprinting approach to show a concurrent shift towards more N_2-fixing cyanobacteria in the phytoplankton community supporting export production over this time period, consistent with the conclusions of Sherwood and co-authors.

Together, these records indicate dramatic responses in both broad algal community structure and fundamental biogeochemical cycles to shifting climate states of the NPSG. Specifically, these data have suggested: 1) direct coupling in major changes of primary production $\delta^{15}N$ and $\delta^{13}C$ values over the last ~1000 years, 2) that present primary production $\delta^{15}N$ and $\delta^{13}C$ values are the lowest in at least a millennia, 3) the variability in $\delta^{15}N$ and $\delta^{13}C$ of export production is driven primarily by algal community structure shifts, and 4) that stratification may be a major driver for these changes in plankton community dynamics (Sherwood et al., 2014; McMahon et al., 2015). However, in order to assess these hypotheses within the broader context of the Holocene, longer records are required to better understand the potential drivers for recent variability and to potentially facilitate predictions of ecosystem responses to future change.

The main goal of this study was to determine if the dramatic changes documented in the last 150 yrs are in fact unique, and if similar coupled $\delta^{15}N$ and $\delta^{13}C$ shifts are typical on millennial timescales. We report bulk stable nitrogen and carbon isotope records extending into the Mid-Holocene (~5000 ybp), from proteinaceous deep-sea coral specimens collected from

offshore Oahu, Hawaii. Proteinaceous deep-sea coral skeletons' bulk $\delta^{15}N$ and $\delta^{13}C$ stable isotope values are a reliable proxy of baseline isotope dynamics represented by source and essential amino acid values (e.g., Schiff et al., 2014; Sherwood et al., 2014; McMahon et al., 2015; 2017). These new records are used to examine the stability of historical baselines in export production $\delta^{15}N$ and $\delta^{13}C$ values.

2. Materials and Methods:

Three sub-fossil *K. haumeaae* deep-sea coral samples were collected from ~400 m depth offshore of Lanikai on the island of Oahu, Hawaii (21° 24.4 N, 157° 38.6 W). We refer to individual specimens as Lanikai 1, 2, and 3 (L1, L2, and L3) in results and discussion below. Skeletons were washed with seawater then fresh water before being air-dried on deck. Cross section disks ~0.7 cm thick were cut from close to the basal attachment, polished, and mounted onto glass plates. A computerized Merchanteck micromill was used to isolate 2-3 mg of proteinaceous coral skeleton at 0.1 mm increments along radial transects from the outer edge to the center.

Bulk $\delta^{15}N$ and $\delta^{13}C$ analyses were conducted on ca. 0.3 mg raw material using a Carlo Erba 1108 elemental analyzer coupled to a ThermoFinningan Delta Plus XP isotope ratio mass spectrometer at the UCSC Stable Isotope Laboratory, following the lab's standard bulk stable isotope protocols (*https://websites.pmc.ucsc.edu/~silab/EA_Protocol.php/*). Results are reported in conventional per mil (‰) notation relative to air and VPDB standards for $\delta^{15}N$ and $\delta^{13}C$, respectively. Standard laboratory error is 0.2‰ for both $\delta^{15}N$ and $\delta^{13}C$, with duplicate coral analyses (n=28) indicating 0.11‰ and 0.14‰ reproducibility for $\delta^{15}N$ and $\delta^{13}C$, respectively.

Radiocarbon analyses were performed on 5-7 acid-pretreated sub-samples per specimen. Age-models were determined for each specimen using Bacon, a Bayesian modeling approach, (Blaauw and Christensen 2011), with Marine13 (Reimer et al., 2013). Isotopic regime shifts were detected using the methodology of Rodionov (2004), with a significance level of 0.1, cut off length of 10, and a Huber's weight parameter of 1. The regime shift program uses a sequential t-test to determine regimes and can detect shifts in both the mean level of fluctuations and the variance (Rodionov 2004).

For comparison with published bulk sediment $\delta^{15}N$ records, cores whose chronology were ^{14}C based were updated using Marine13 (Reimer et al., 2013; details in Supplementary file). $\delta^{15}N$ records from the NICOPP database (Tesdal et al., 2013) were standardized to a mean of zero for the last 6000 years and datasets were combined to analyze a regional, composite response (Fig. S3, S4). Sediment records were restricted to those that had more than two $\delta^{15}N$ sampling points in the last six millennia. Simple bivariate linear regressions were performed using JMP Pro® version 12 on both coral and sediment records to examine long-term trends and probabilities.

3. Results:

3.1 Timescale and resolution

The 95% confidence interval for the individual age models averaged 98 ± 15 years (Fig. S1, Table S1). The L1 record (1510 to 220 CE) partially overlaps with the coral record from an adjacent location in Sherwood et al. (2014) but extends the record by nearly 1000 years. L1 had

an estimated average radial growth rate of 14 μm yr^{-1}, such that that isotope samples averaged 7 yrs. The L2 coral spanned ~565 years from -20 to -580 CE, with a growth rate of 21 μm yr^{-1} and isotope data averaging 5 yrs. L3 was the oldest coral and spanned ~1420 years from -1540 to -2960 CE. L3 had an estimated growth rate of 19 μm yr^{-1}, with isotope data averaging 5 yrs.

3.2 Stable Isotope Results

Stable isotope data and C:N ratios as a function of radial distance and age are reported in Supplementary Table S2.

3.3 Nitrogen Stable Isotopes

L1 $\delta^{15}N$ values overlap data from a specimen from nearby Makapu'u, presented in Sherwood et al., (2014), for nearly 300 yrs (Fig. 2A). L1 $\delta^{15}N$ values range ~2‰ from a low of 8.8‰ in 240 CE to a high of 10.8‰ in 1440 CE. There appear to be $\delta^{15}N$ oscillations around an average of 9.4 ± 0.3‰ (n=82) between 220 CE and 580 CE, followed by a large increase of ~1.2‰ from 660 CE to a high of 10.3‰ in 680 CE. $\delta^{15}N$ values then decline to an average of 9.9 ± 0.2‰ (n=66) between 710 CE and 1260 CE, followed by an increase of ~0.7‰ over the next two decades to a new stable period with average values of 10.6 ± 0.2‰ (n=29) from 1280 CE until the coral's death in 1510 CE.

The L2 coral (-20 to -580 CE) exhibits no clear secular trend but has substantial oscillations (range ~1.6‰) about the mean $\delta^{15}N$ value of 9.2 ± 0.3‰ (n=120). The end of the L2 record (-20 CE) matches within error of the start of L1 300 years later. Regime detection (Fig. S2) notes periods of high $\delta^{15}N$ values during -420 to -450 CE (9.8 ± 0.2‰, n=6) as well as -300

to -340 CE (9.5 ± 0.1‰, n=10). The highest $\delta^{15}N$ value was 10.0‰ (-430 CE). There was a drop in $\delta^{15}N$ values between -190 and -100 CE to an average of 8.8 ± 0.4‰ (n=18), and the lowest $\delta^{15}N$ value was 8.4‰ in -180 CE.

The Mid-Holocene L3 coral (-1540 to -2960 CE) has substantially more positive $\delta^{15}N$ values (10.8 ± 0.3‰, n=251) compared to all the Late-Holocene and near modern coral data (Fig. 2A). From -2940 to -2600 CE there is an interval where $\delta^{15}N$ increases (0.02‰ decade^{-1}, R^2 = 0.51, $p < 0.0001$) from 10.3‰ to 10.9‰, despite reaching its lowest value of 10.0‰ in a brief excursion near -2720 CE. There is also an apparent step change of ~0.5‰ that occurs around -2300 CE as values increase from 10.7 ± 0.1‰ (-2390 to -2280 CE, n=18) to 11.2 ± 0.2‰ (-2270 to -2100 CE, n=34). After this, values once again return to the coral's overall average, except for a ~90 year regime of higher values (11.1 ± 0.2‰, n=20) between -1940 and -1840 CE (Fig. S2).

3.4 Carbon Isotope Results

We observe a ~2‰ total range in coral $\delta^{13}C$ values, with low $\delta^{13}C$ values very similar to present day occurring multiple times since the Mid-Holocene (in L1 ~200 CE; in L2 ~800 BCE; in L3 ~2800 BCE). L1 coral $\delta^{13}C$ values ranged over 1.5‰ (Fig. 3A), with $\delta^{13}C$ increasing towards the present**.** As with the L1 $\delta^{15}N$ records, there is a significant overlap between the L1 coral $\delta^{13}C$ record and previously published Makapu'u $\delta^{13}C$ records (McMahon et al., 2015). L1 $\delta^{13}C$ values begin low at -17.1 ± 0.1‰ (n=43) between 220 - 460 CE, before increasing by ~0.4‰ over the next few decades to an average of -16.7 ± 0.1‰ (n=119) from 480 to 1380 CE. Values then rapidly increase by ~1‰ (0.06‰ decade^{-1}, R^2 = 0.85, $p < 0.0001$), to reach the highest value of -15.8‰ in 1530 CE at the coral's death.

The L2 $\delta^{13}C$ values range by ~1.0‰ over the length of the ~565 year record (Fig 3A). However, in contrast with the relatively stable $\delta^{15}N$ record the L2 $\delta^{13}C$ record increases by 1.4‰ through this time period (average change of 0.01‰ decade^{-1}, $R^2 = 0.54$, $p < 0.0001$). The $\delta^{13}C$ values ranged from -15.5‰ (-90 CE) to -16.9‰ (-370 CE), and as a whole the L2 record indicates a large isotopic discontinuity in export production $\delta^{13}C$ values from the end of L2 to the more recent L1 $\delta^{13}C$ record.

The Mid-Holocene L3 record (-1540 to -2960 CE) is also marked by a large and statistically significant, nearly unidirectional, shift of ~2‰ in $\delta^{13}C$ values (0.01‰ decade^{-1}, $R^2 = 0.85$, $p<0.0001$), ranging from -15.2‰ (-1540 CE) to -17.2‰ (-2860 CE) (Fig 3A). Regime detection suggests this increase occurred between plateaus of more constant values, rather than strictly linearly (Fig. S2). Based on regime detection periods, L3 averages -16.6 ± 0.1‰ (n=49) between -2680 to -2300 CE, increases to -16.3 ± 0.1‰ (-2290 to -2080 CE, n=41), reached a third plateau of -15.8 ± 0.1‰ (-1940 to -1630 CE, n=64), before finally increasing until the record end (Fig. S2). The transition between plateaus around -2300 CE is also coincident with a similar change in $\delta^{15}N$ values. In addition, a sharp drop and apparent recovery of $\delta^{13}C$ values of ~0.4‰ is observed near the early part of the record around -2850 CE.

3.5 Coupling vs. Decoupling of Nitrogen and Carbon Isotope Records

The combined isotope records show several distinct periods of coupling where $\delta^{13}C$ and $\delta^{15}N$ values trend similarly, corresponding closely to what has been observed in records from this region in the last millennium. However, equally common in the longer Holocene records are

periods where $\delta^{13}C$ and $\delta^{15}N$ variability is decoupled, with either little change in one isotope record corresponding to strong change in the other, or else measured or inferred $\delta^{13}C$ and $\delta^{15}N$ records which trend in opposite directions. Unlike the most recent ~1400 years where $\delta^{13}C$ and $\delta^{15}N$ are coupled, for more than a thousand years (-580 to 670 CE) the $\delta^{13}C$ and $\delta^{15}N$ values are generally decoupled, suggesting a different regime than modern (Fig. 4, "DC1", representing L2 and part of L1 corals). As noted previously, the $\delta^{15}N$ values throughout this same period (-580 to 670 CE, including the gap between L1 and L2 records) remained relatively constant (mean of 9.3 ± 0.3‰), while in contrast the $\delta^{13}C$ values increased in L1 and L2 corals (from -430 to -20 CE and 250 to 670 CE), with an additional large decline in $\delta^{13}C$ values (~1‰) required to connect values between these two records. Further back in the ~1000 year period between L3 and L2 (Fig. 4, "C2"), the offset between coral records indicates an overall shift in both $\delta^{15}N$ and $\delta^{13}C$ to much lower values from past to present. The Mid-Holocene trends in $\delta^{13}C$ and $\delta^{15}N$ values appear to have become decoupled once again from -2550 to -1540 CE, with $\delta^{15}N$ values averaging 10.9 ± 0.3‰, while $\delta^{13}C$ values increase by ~1.5‰. Finally, in the earliest part of these coral records (-2950 to -2550 CE), both $\delta^{15}N$ and $\delta^{13}C$ values again trend in the same direction.

4. Discussion

4.1 Nitrogen Isotopic Records

The records exhibit a surprisingly wide range in $\delta^{15}N$ values of about 3.5‰, marked by several distinct regimes, with the most positive $\delta^{15}N$ values seen in the Mid-Holocene and lowest in the present day (Fig. 2). Using this new 5000 yr $\delta^{15}N$ dataset for context, it is clear that the rate of the post-1850 decline (1.5‰ in 150 yrs) is significant and unique. More common in the

coral data are long periods of relative stability, with millennial-scale plateaus of similar $\delta^{15}N$ values in three intervals (from approximately -2960 to -1540 CE, -580 to 660 CE, and from 660 to the 1800s; Fig. 2). While there is no direct coral data for the millennial-scale gap from -1530 to -580, the offset between L2 and L3 indicates that a ~1.5‰ shift in $\delta^{15}N$ must have occurred in this period. If this inference is correct, this would represent a shift in $\delta^{15}N$ value of export production similar in magnitude to the change in the last 150 years, but potentially over 1000 years (Fig. 2).

Since nitrate is fully utilized on an annual scale in the NPSG, isotope mass balance requires that the overall $\delta^{15}N$ value of autotrophs represents an integrated signal of the $\delta^{15}N$ value of their nitrogen sources. Thus, gyre-based paleo-$\delta^{15}N$ records can be interpreted in terms of the relative balance of isotopically distinct nutrient sources supporting export production (e.g., Altabet et al. 2006; Dore et al. 2002; Sherwood et al 2014). The large ~3.5‰ variability in $\delta^{15}N$ values recorded in these corals could therefore be driven by either changing phytoplankton communities (i.e., relative importance of diazotroph N_2-fixation), and/or shifts in the source $\delta^{15}N$ value of advected nitrate. This latter aspect includes both the water mass being entrained during mixing as well as $\delta^{15}N_{NO3}$ values sourced from the margins. Both situations could have been influenced by changes in water column stability and ocean-biogeochemistry dynamics.

In the NPSG near the Hawaiian islands nitrogen fixation leads to characteristically low $\delta^{15}N$ values (~0‰) in the upper euphotic zone, while mesopelagic nitrate sources have much higher values (Dore et al., 2002; Casciotti et al., 2008). By assuming mass balance based on a two-component mixing model, with $\delta^{15}N_{N2\text{-}fix}$ = 0‰ and $\delta^{15}N_{NO3}$ = 6.5‰, and a sinking

280 particulate bulk $\delta^{15}N$ value of 3.5 ± 0.2‰ at 300 m (Casciotti et al., 2008; Dore et al., 2002; Karl
281 et al., 1997), around half (~46%) of present-day exported production is supported by N_2 fixation.
282 The amino acid phenylalanine $\delta^{15}N_{phe}$ values in Hawai'ian proteinaceous corals have been used
283 as a proxy for baseline nitrate and average 2.5 ± 0.3‰ over the late 20th and early 21st century
284 (n=7; Sherwood et al., 2014; McMahon et al., 2017), which implies a similar, albeit slightly
285 higher (~60%) fraction of export production supported by nitrogen fixation. As documented by
286 Sherwood et al., 2014, there is a very strong 1:1 relationship (R^2 = 0.77) between bulk skeleton
287 $\delta^{15}N$ and $\delta^{15}N_{phe}$ in *K. haumeaae.* Assuming that this 1:1 covariance is maintained in these
288 specimens, it is possible to directly transform (interpret) changes in bulk coral $\delta^{15}N$ into baseline
289 variability.
290
291 Water column denitrification discriminates strongly against the heavier ^{15}N isotope,
292 leaving seawater nitrate more positive in ^{15}N, and ocean circulation patterns can transport this
293 isotopic signal throughout the Pacific (Altabet, 2006; Sigman et al., 2009). Analysis of North
294 Pacific sediment records (n=30) indicates an overall decline of ~0.5‰ in bulk sediment $\delta^{15}N$
295 values since the Mid-Holocene (Fig. S3, S4). The decline in sedimentary $\delta^{15}N$ is assumed to
296 reflect changes in overlying nitrate values and has been attributed to a decline in water column
297 denitrification through the Holocene (Jia and Li, 2011 and references therein). However, a
298 gradual ~0.5‰ decline in whole North Pacific Ocean $\delta^{15}N_{NO3}$ values clearly cannot be the
299 primary driver of $\delta^{15}N$ values in our coral records, which exhibit significant variability in $\delta^{15}N$
300 values rather than monotonic changes. There is also little variability in sedimentary $\delta^{15}N$ values
301 from source regions of the Eastern Pacific that intersect water-masses (isopycnals) ventilating the
302 NPSG interior (Fig. 2C), which corresponds to variability in $\delta^{15}N$ export production as

303 reconstructed by coral data. We are thus left with two potential mechanisms that drive the
304 variability we observe. The first is a change in plankton community structure with variable
305 importance of nitrogen fixing diazotrophs and the second is a change in the source of water being
306 entrained into the mixed layer that provides nitrate to the NPSG. It is likely that the physical
307 forcing for these two aspects is related: a more stratified ocean has diminished input from deeper
308 water masses and could provide an expanded niche for diazotrophs (Karl et al., 2001; McMahon
309 et al., 2015).
310
311 Mid-Holocene $\delta^{15}N$ values from the L3 specimen average 10.8‰ with sustained positive
312 values in excess of 11‰. Within the context of the modern endmember model previously
313 discussed, a value of 11‰ implies that ~80% of the export production is supported by subsurface
314 nitrate (ie., only ~20% supported by nitrogen fixation). Specimens L3 and L2 (-1530 to -580 CE)
315 would suggest an increase in the contribution of N_2-fixation to export production across this gap
316 with the source apportionment reaching close to equal. From ~580 BCE to the beginning of the
317 Little Ice Age (~1450 CE), a return to production supported more by nitrate (~70%) than
318 nitrogen fixation (~30%) appears likely. If the entrained nitrate was sourced from deeper in the
319 water column, the apportionment difference between NO_3^- and N_2-fixation would become less.
320 That being said, the data require 1) simply a higher concentration of NO_3^- sourced from similar
321 present-day depth, 2) more positive $\delta^{15}N_{NO3}$ entrained from deeper isopycnals or 3) a different
322 source origin. Deepening of the mixed-layer due to cooling and/or more frequent storm events
323 (windiness) is an obvious mechanism to reduce stratification and increase the vertical flux of
324 NO_3^- into the mixed-layer. In the modern NPSG, stratification is the most common underlying
325 driver associated with shifts in diazotroph communities and rates of nitrogen fixation (Karl et al.,

2001). Increased rates of N_2-fixation with abundant populations of *Trichodesmium* have been found to occur during the warm phase of El Niño Southern Oscillation (ENSO; Karl et al., 1995; Corno et al., 2007) when persistent subsidence leads to decreased cloud cover, rainfall, and storminess in the Hawai'ian Islands (Chu and Chen, 2005; Diaz and Giambelluca, 2012.). A coupling of warm sea surface temperatures and increased stratification is likely associated with less cloudiness and reduced storminess, which should correspond to lower $\delta^{15}N$ values. Thus, on millennial timescales, the balance of nitrogen supporting export production likely reflects the large-scale circulation associated with the migration of the descending limb of the Hadley Cell and the Intertropical Convergence Zone (ITCZ) that follows summer insolation (Fig. 2).

Solar forcing influences the position of the ITCZ by modulating its latitudinal extent, with a concomitant influence on ENSO variability (Clement et al., 2000; Schneider et al., 2014; Lu et al., 2018). Sediment data suggests $\delta^{15}N$ varies by latitude, with more positive $\delta^{15}N$ values (~2.5‰) offshore of Mexico in comparison to near the equator (Fig. 2C). A southward shift of the ITCZ is expected to enhance equatorial upwelling (Schneider et al., 2014). On millennial timescales when the ITCZ is more southward during the Late-Holocene, it may be that comparatively more negative $\delta^{15}N$ waters are advected to the NPSG. While there are some discrepancies between ENSO proxy records due to sparse data sampling and proxy-record specific assumptions, there is general agreement on a reduction in interannual ENSO variability, including amplitude, 4-5 kyrs BP and increases in ENSO variability between 1-2 kyrs BP (Lu et al., 2018 and references therein). Although our records are too coarse to capture interannual variability, we can explore the multidecadal variability that impacts SSTs and storminess (precipitation) in the Hawai'ian Islands (Karl et al. 1995; Chu and Chen, 2005; Diaz and

Giambelluca, 2012). Spectral analysis did not reveal consistent multi-decadal to centennial scale power in the Lanikai data and while the detected regimes (n=29) did not often overlap in timing between $\delta^{15}N$ and $\delta^{13}C$ records (Fig. S2), most regimes (~60%) tended to last between 30 and 90 years in duration. We posit that the regime analysis is confirming multi-decadal variability, but the mechanistic forcing cannot yet be precisely elucidated.

4.2 Carbon Isotopic Records

The ~2‰ range in coral $\delta^{13}C$ values across our 5000 yr record also appear to occur within a number of discrete cycles in $\delta^{13}C$ values of export production, with low $\delta^{13}C$ values similar to present day having occurred multiple times since the Mid-Holocene (in L1 ~ 200 CE; in L2 ~ 800 BCE; in L3 ~ 2800 BCE). Bulk coral $\delta^{13}C$ values have a strong, positive relationship with essential amino acid $\delta^{13}C$ values in *K. haumeaae*, particularly the $\delta^{13}C$ value of phenylalanine (R^2=0.69, McMahon et al. 2015), which indicates that most bulk $\delta^{13}C$ variability can be tied to changes in the source carbon at the base of the food web. However, it should be noted that variations in bulk $\delta^{13}C$ values are typically muted in magnitude compared to the $\delta^{13}C$ signal from essential amino acids (Schiff et al. 2014; McMahon et al., 2015), thus suggesting bulk coral $\delta^{13}C$ records may underestimate the full extent of variability in baseline export changes.

There are multiple factors influencing planktonic $\delta^{13}C$ values in the marine environment, but on long timescales the dominant controls include SST, ambient CO_2 (aq.) concentrations, the $\delta^{13}C$ of dissolved organic carbon (DIC), and taxon-specific fractionation values (ε_f) (Rau et al., 1996; Young et al., 2013; McMahon et al., 2015). Given that these factors can be inter-linked,

definitively assigning causes to past changes in export production $\delta^{13}C$ values is challenging. Consideration of both past paleo-reconstructions and modern experiments on the effects of main physical forcings (temperature, pCO_2, atmospheric $\delta^{13}C$) can help to refine potential interpretations. Increased CO_2 availability, whether through increased external CO_2 concentrations or increases in [DIC], generally results in decreased $\delta^{13}C$ values and a greater discrimination between the phytoplankton and source CO_2 (Rau et al., 1989; Young et al., 2013). However, from the Mid-Holocene to the Little Ice Age, the concentration of CO_2 in the atmosphere has increased by only ~10 ppm, with little to no change in atmospheric $\delta^{13}C$ (fig. 3; Monnin et al., 2004), suggesting that the signal being recorded in these corals is not mainly due to pCO_2 change. The low sensitivity of plankton $\delta^{13}C$ to changes in pCO_2 (0.0003‰ ppm^{-1};, Young et al. 2013) would further indicate that atmospheric $\delta^{13}C$ value is not a main driving mechanism for the large changes in our coral records. Baseline changes in the $\delta^{13}C$ of DIC are also likely to be too small to be driving the trends in coral $\delta^{13}C$ (Quay and Stutsman, 2003; Monnin et al., 2004).

Laboratory and field experiments document that temperature exerts a significant control on phytoplankton and exported organic matter $\delta^{13}C$ values (Table S3, and associated references). In general, warmer conditions contribute to more positive exported organic $\delta^{13}C$ values. Multiple approaches have attempted to quantify the effects of temperature on the $\delta^{13}C$ values of primary production, including: estimates of the effect of temperature on fractionation factors in culture (ε_p; +0.12‰/°C) and on phytoplankton $\delta^{13}C$ (+0.11-0.23‰/°C) and suspended particulate organic carbon $\delta^{13}C$ (+0.41‰/°C) in natural ocean systems. Mid- to Late-Holocene SST estimates using both the Modern Analog Technique and alkenone-SST relationships in sediment

cores near Oahu indicate temperatures within 1°C of early 20th century data (Lee et al., 2001). These estimates are similar to higher resolution Northern Hemisphere reconstructions (e.g., Pei et al. 2017). A ≤1°C SST change would only account for ~0.4‰ or less of the 2‰ $\delta^{13}C$ variability, suggesting temperature alone is only partially responsible for the trends in coral $\delta^{13}C$.

Shifting plankton community composition, implicitly including size/morphology and growth rate, is the most likely explanation for the large changes in $\delta^{13}C$ values of our coral records over the last 5000 yrs. Different phytoplankton species have unique carbon isotope fractionations during photosynthesis (Laws et al., 1995; Rau et al., 1996), and thus a shifting phytoplankton community composition can be a major driver behind changes in $\delta^{13}C$ of export production over time (McMahon et al., 2015). Prokaryotic cyanobacteria (e.g., *Prochlorococcus, Synechococcus*) and picoeukaryotes are typically the dominant phytoplankton groups in open ocean regions like the NPSG (e.g., Karl et al., 2001), and of these, *Synechoccocus* and picoeukaryotes are most strongly associated with carbon export in oligotrophic regions (Guidi et al. 2016). Picoeukaryotes are also larger than prokaryotes (cell diameters of 2.0 and 0.5 μm respectively) and this contributes to differences in their ecological performance as well as the extent of carbon fixation and export (Massana and Logares 2013). Based on distinct isotopic fractionations associated with enzymatic, intracellular carbon fixation (ε_f ; Laws et al., 1995; Scott et al., 2007), the differences between prokaryotic and eukaryotic contributions to exported organic matter manifest as differences in $\delta^{13}C$ values: where ~0.6‰ of $\delta^{13}C$ variability can be explained by a 1‰ shift in community fractionation ε_f (Table S3). More positive $\delta^{13}C$ values indicate higher relative contributions of eukaryotic phytoplankton, consistent with the well-

417 known general trend that larger phytoplankton cells (e.g. diatoms) express more positive $\delta^{13}C$
418 values than small-celled nanoplankton (e.g., Laws et al., 1995; Popp et al. 1998).
419
420 Coral $\delta^{13}C$ values suggest centennial to millennial scale trends towards increasing
421 eukaryotic contributions in exported production followed by hypothesized events (e.g. between
422 L3 and L2) that reset the NPSG to be more prokaryotic-dominated. Picoeukaryotes are
423 metabolically less flexible than prokaryotic organisms, perhaps causing them to be less resilient
424 to environmental changes (Massana and Logares, 2013). Prokaryotic CO_2 fixers also outgrow
425 and outperform eukaryotes in oligotrophic gyre ecosystems (Zubkov 2013), which suggests that
426 during periods of stratified, nutrient-limited conditions, prokaryotic organisms may dominate
427 primary production and thus export production in the NPSG. The stability of the water column
428 due to the frequency of ENSO events may influence community structure, with periods of low
429 ENSO activity (e.g., ~3.5-5 kyrs ago) allowing for a long term community increase of eukaryotic
430 organisms. This would result in the observed steadily increasing $\delta^{13}C$ values of coral L3), while
431 periods of high ENSO activity (e.g. 1-2 kyrs ago and 3-4 kyrs ago; Moy et al. 2002, Fig. 3)
432 would correspond to a community consistently dominated by prokaryotes and low, stable $\delta^{13}C$
433 values (averaging -16.9 ± 0.2‰ from 200 to 1000 CE, Fig. 3). Shifts between smaller celled
434 prokaryotes and larger picoeukaryotes can modulate the amount of organic matter exported to
435 depth and may cause cascading effects on pelagic and benthic food webs (Finkel et al. 2010).
436

437 **4.3 Coupling vs. Decoupling of export production $\delta^{15}N$ and $\delta^{13}C$ values**

438 Existing records from deep-sea corals from the NPSG in the last 1000 yrs have uniformly
439 documented coupled changes in $\delta^{15}N$ and $\delta^{13}C$ values at the base of the food web, with authors

hypothesizing that such shifts are linked to recent shifts in local/regional temperature and the ecosystem response derived from the dynamical oceanographic setting coincident with warmer surface temperatures (e.g., Sherwood et al., 2014; McMahon et al., 2015). Therefore, the observation that in the longer Holocene record, relative changes in $\delta^{15}N$ and $\delta^{13}C$ values of export production often trend in *opposite* directions was unexpected. The $\delta^{15}N$ and $\delta^{13}C$ data from these coral specimens, including the required changes necessary to bridge gaps between records, clearly indicate three periods in which changes in $\delta^{15}N$ and $\delta^{13}C$ values are largely synchronous (moving in the same direction, with generally similar slopes), and two periods in which values appear decoupled (Fig. 4; *Results* 3.5). This suggests a more complex set of biogeochemical forcings on the longer time scales of these records.

In all coral records for the last millennium, the direct coupling between $\delta^{15}N$ and $\delta^{13}C$ shifts is one of the most striking overall features (Fig. 4). This observation supports the conclusion that regional plankton community changes are the underlying driver for changes observed in isotope records, primarily reflecting shifts between a more stable water column promoting oligotrophic and N_2-fixation conditions versus cooler periods with increased vertical mixing and entrainment (Sherwood et al., 2014; McMahon et al., 2015). Specifically, more recent warmer periods are characterized by more stratified and nutrient-poor conditions with enhanced nutrient recycling and fewer large eukaryotic cells (e.g., Chavez et al., 2011). Such conditions favor microbial-loop dominated systems characterized by lower $\delta^{13}C$ values. The enhanced N_2-fixation and nutrient recycling in such systems also leads to lower $\delta^{15}N$ values, accounting for linked $\delta^{15}N$ and $\delta^{13}C$ changes. Conversely, higher nutrient environments are

462 typified by faster growing, larger eukaryotic autotrophs supported by upwelled nitrate, leading to
463 concurrent increases in both $\delta^{15}N$ and $\delta^{13}C$ primary production values.
464
465 The decoupling of $\delta^{15}N$ and $\delta^{13}C$ changes in earlier periods of this ~5000 yr record
466 suggest distinctly different local to basin-scale drivers for $\delta^{15}N$ and $\delta^{13}C$ values. While earlier
467 data indicate several periods of coupled $\delta^{15}N$ and $\delta^{13}C$ change in the NPSG that appear to be
468 analogues to the recent millennium, the distinct periods of coupling and decoupling must indicate
469 different mechanisms are driving changes in primary production N and C cycles. The two
470 periods of *decoupled* isotopic behavior (Fig. 4, DC1, DC2) occur when hemispheric
471 temperatures may have been ~0.5° cooler than present (Pei et al., 2017) and proxy records
472 suggest reduced ENSO climate variability (Lu et al. 2018; Moy et al. 2002). In contrast, the
473 coupled period C1 includes the warmer Industrial Revolution and Medieval Climate Anomaly
474 where proxy records agree on enhanced ENSO conditions (Lu et al. 2018 and references therein),
475 while the C2 period roughly corresponds to the end of northern hemisphere neoglaciation. Both
476 C2 and C3 occur during enhanced ENSO activity periods as characterized by some proxy records
477 (e.g. Moy et al. 2002, Fig 3). One hypothesis for this apparently contrasted behavior is that
478 coupling versus decoupling may be related to relative regional sea surface temperatures and
479 stratification. Cooler periods of reduced ENSO variability are decoupled in $\delta^{15}N$ and $\delta^{13}C$ values,
480 while warmer, enhanced ENSO periods are more consistently coupled. While speculative, this
481 could be due to changing nutrient regimes. Generally warmer SSTs correspond to enhanced
482 ocean stratification, shallower mixed layer depths, and a slowdown in gyre circulation. Under
483 such oligotrophic conditions, phytoplankton communities may rely more heavily on the supply
484 of N_2-fixed nitrate from localized diazotroph production, and community composition may shift

485 towards prokaryotic, N_2-fixing organisms, perhaps causing a coupling in $\delta^{13}C$ and $\delta^{15}N$ values of
486 export production. In contrast, there is both more mixing from depth and/or enhanced lateral
487 advection of water from ocean margins during cooler, often windier, climatic periods (Sigman et
488 al. 2009). The result is lower rates of N_2-fixation (Galbraith et al., 2004) and more nitrate with
489 more positive $\delta^{15}N$ values possibly advected from higher latitudes of the Eastern Pacific. Thus,
490 community composition changes may serve to shift $\delta^{13}C$ values, while the signal of advected
491 $\delta^{15}N_{NO3}$ and not N_2-fixation drives the $\delta^{15}N$ value of exported organic matter during periods of
492 cooler SSTs, thus decoupling the $\delta^{13}C$ and $\delta^{15}N$ values. McMahon and coauthors (2015) supports
493 this idea, suggesting nitrate utilizing cyanobacteria dominate community composition over some
494 periods while N_2-fixating cyanobacteria dominate over others during the most recent millennium.
495 While this idea cannot be directly tested using bulk isotope analysis, further work could address
496 it.
497
498 **5. Conclusions**
499 This study documents variability in export production $\delta^{15}N$ and $\delta^{13}C$ values for the
500 Holocene NPSG, extending previously published records by approximately ~4000 years deeper
501 into the Mid-Holocene. These new data reveal a dynamic biogeochemical system, in which
502 substantial changes in $\delta^{15}N$ and $\delta^{13}C$ values of export production have been common on
503 millennial time scales. Our records indicate that the natural (preindustrial era) isotopic range of
504 production in the NPSG has varied by up to 3.5‰ for $\delta^{15}N$ values and 2‰ for $\delta^{13}C$ values over
505 the last 5000 yrs. In particular, Mid-Holocene export production $\delta^{15}N$ values appear to have been
506 substantially higher (by ~1.5 to 2‰) than in the Late-Holocene, and these longer records confirm
507 that present day $\delta^{15}N$ values recorded in corals (~8‰) are the lowest in ~5000 years. In contrast,

low $\delta^{13}C$ values similar to those recorded in modern corals (~ -17‰) were reached during at least two other periods since the Mid-Holocene.

While these data clearly show periods of major change in both $\delta^{15}N$ and $\delta^{13}C$ values over the last 5000 years similar in magnitude to changes in the Anthropocene, past changes appear to have occurred over much longer (~millennial) timescales. In addition, these new records also indicate that distinct periods of coupled and decoupled $\delta^{15}N$ and $\delta^{13}C$ dynamics occurred in different periods throughout the Holocene. This in turn suggests a number of independent biogeochemical regimes over the last 5000 yrs. We hypothesize that these regimes are most likely linked to shifts in plankton community structure, possibly coupled with independently varying $\delta^{15}N$ values of nitrate in this region. The coupled $\delta^{15}N$ and $\delta^{13}C$ periods are similar to shifts observed in both NPSG instrumental records and also in more recent coral chronologies, likely explained by relative importance of nitrogen fixation and upper water stratification (McMahon et al., 2015; Sherwood et al., 2014). Periods in which $\delta^{13}C$ values change with no major shifts $\delta^{15}N$ values imply changes in phytoplankton community structure without clear linkage to shifts in nutrient supply, potentially explained by relative abundance of non-nitrogen fixing prokaryotic autotrophs in this region (McMahon et al. 2015). However, to test these ideas more work will be necessary to identify the relative influence of baseline nutrient supply vs. changes in autotrophic community structure.

Overall, the dynamism of Holocene biogeochemical systems revealed by this study strongly emphasizes the need to develop new proxies that can be used to determine past climate and environmental conditions at high resolution in the NPSG. Future work should include

compound specific analysis of amino acids within coral archives to further constrain these hypotheses. Such information would allow researchers to directly examine if present microbial-loop dominated system of the NPSG has been constant or if variation in community structure has been responsible for isotopic variability of our records earlier in the Holocene. Further, this approach would allow for testing of the underlying assumption that average trophic structure of NPSG planktonic systems, which strongly influences the $\delta^{15}N$ value of export production, has remained constant through time. While data from Sherwood et al. (2014) indicated that average planktonic ecosystem trophic position has remained constant over the most recent millennium, it is not known if this also would hold true for earlier parts of this record, specifically during periods of $\delta^{13}C$ and $\delta^{15}N$ decoupling. Regardless, we show that while NPSG plankton and nutrient dynamics are highly variable over the last 5000 yrs, the modern anthropoence regime remains unique in the magnitude and timing of changes in ecosystem dynamics in the context of Holocene variability.

Acknowledgements:

None of this work would have been possible without the captain and crew of the RV *Ka'imikai-o-Kanaloa* and the pilots and engineers of the Hawaii Undersea Research Lab's Pisces IV and V. Sample collection was funded by NOAA/NURP and the National Geographic Society (7717-04). A portion of this work was performed under the auspices of the U.S. Department of Energy (DE-AC52-07NA27344). The majority of the work presented here was funded by the NSF (OCE 1061689). D.S. Glynn was supported by a Cota Robles and NSF GRFP Fellowship. Further thanks go to D. Andreasen, C. Carney, R. Franks, and J. Schiff for laboratory assistance and training.

References:

Altabet, M.A., 2006. Isotopic Tracers of the Marine Nitrogen Cycle: Present and Past. Hdb Env Chem 2, 251–293. https://doi.org/10.1007/698_2_008

Berger, A., Loutre, M.F., 1991. Insolation values for the climate of the last 10 million years. Quat. Sci. Rev. 10, 4, 297-317. https://doi.org/10.1016/0277-3791(91)90033-Q

Blaauw, M., Christen, J.A., 2011. Flexible paleoclimate age-depth models using an autoregressive gamma process. Bayesian Anal. 6, 457–474. https://doi.org/10.1214/11-BA618

Boyce, D.G., Lewis, M.R., Worm, B., 2010. Global phytoplankton decline over the past century. Nature 466, 591–596. https://doi.org/10.1038/nature09268

Casciotti, K.L., Trull, T.W., Glover, D.M., Davies, D., 2008. Constraints on nitrogen cycling at the subtropical North Pacific Station ALOHA from isotopic measurements of nitrate and particulate nitrogen. Deep. Res. Part II Top. Stud. Oceanogr. 55, 1661–1672. https://doi.org/10.1016/j.dsr2.2008.04.017

Chavez, F.P., Messié, M., Pennington, J.T., 2011. Marine primary production in relation to climate variability and change. Ann. Rev. Mar. Sci. 3, 227–260. https://doi.org/10.1146/annurev.marine.010908.163917

Chu, P.S., Chen, H., 2005. Interannual and interdecadal rainfall variations in the Hawaiian Islands. J. Clim. 18, 4796–4813. https://doi.org/10.1175/JCLI3578.1

Clement, A.C., Seager, R., Cane, M.A., 2000. Suppression of El Niño during the Mid-Holocene by changes in the Earth's orbit. Paleoceanography 15, 731–77. https://doi.org/10.1029/1999PA000466

Corno, G., Karl, D.M., Church, M.J., Letelier, R.M., Lukas, R., Bidigare, R.R., Abbott, M.R.,

2007. Impact of climate forcing on ecosystem processes in the North Pacific Subtropical Gyre. J. Geophys. Res. 112, 1–14. https://doi.org/10.1029/2006JC003730

Di Lorenzo, E., Schneider, N., Cobb, K.M., Franks, P.J.S., Chhak, K., Miller, J., McWilliams, J.C., Bograd, S.J., Arango, H., Curchitser, E., Powell, T.M., Rivière, P., 2008. North Pacific Gyre Oscillation links ocean climate and ecosystem change. Geophys. Res. Lett. 35, 2–7. https://doi.org/10.1029/2007GL032838

Diaz, H.F., Giambelluca, T.W., 2012. Changes in atmospheric circulation patterns associated with high and low rainfall regimes in the Hawaiian Islands region on multiple time scales. Glob. Planet. Change 98–99, 97–108. https://doi.org/10.1016/j.gloplacha.2012.08.011

Dore, J.E., Brum, J.R., Tupas, L.M., Karl, D.M., 2002. Seasonal and interannual variability in sources of nitrogen supporting export in the oligotrophic subtropical North Pacific Ocean. Limnol. Oceanogr. 47, 1595–1607. https://doi.org/10.4319/lo.2002.47.6.1595

Ehrlich, H., Etnoyer, P., Litvinov, S.D., Olennikova, M.M., Domaschke, H., Hanke, T., Born, R., Meissner, H., Worch, H., 2006. Biomaterial structure in deep-sea bamboo coral (Anthozoa: Gorgonacea: Isididae): perspectives for the development of bone implants and templates for tissue engineering. Materwiss. Werksttech. 37, 552–557. https://doi.org/10.1002/mawe.200600036

Finkel, Z. V., Beardall, J., Flynn, K.J., Quigg, A., Rees, T.A. V, Raven, J.A., 2010. Phytoplankton in a changing world: Cell size and elemental stoichiometry. J. Plankton Res. 32, 119–137. https://doi.org/10.1093/plankt/fbp098

Galbraith, E.D., Kienast, M., Pedersen, T.F., Calvert, S.E., 2004. Glacial-interglacial modulation of the marine nitrogen cycle by high-latitude O_2 supply to the global thermocline. Paleoceanography 19, 1–12. https://doi.org/10.1029/2003PA001000

Guidi, L., Chaffron, S., Bittner, L., Eveillard, D., Larhlimi, A., Roux, S., Darzi, Y., Audic, S., Berline, L., Brum, J.R., Coelho, L.P., Espinoza, J.C.I., Malviya, S., Sunagawa, S., Dimier, C., Kandels-Lewis, S., Picheral, M., Poulain, J., Searson, S., Stemmann, L., Not, F., Hingamp, P., Speich, S., Follows, M., Karp-Boss, L., Boss, E., Ogata, H., Pesant, S., Weissenbach, J., Wincker, P., Acinas, S.G., Bork, P., De Vargas, C., Iudicone, D., Sullivan, M.B., Raes, J., Karsenti, E., Bowler, C., Gorsky, G., 2016. Plankton networks driving carbon export in the oligotrophic ocean. Nature 532, 465–470. https://doi.org/10.1038/nature16942

Guilderson, T.P., McCarthy, M.D., Dunbar, R.B., Englebrecht, A., Roark, E.B., 2013. Late Holocene variations in Pacific surface circulation and biogeochemistry inferred from proteinaceous deep-sea corals. Biogeosciences 10, 6019–6028. https://doi.org/10.5194/bg-10-6019-2013

Jia, G., Li, Z., 2011. Easterly denitrification signal and nitrogen fixation feedback documented in the western Pacific sediments. Geophys. Res. Lett. 38, L24605, 1-4. https://doi.org/10.1029/2011GL050021

Karl, D.M., Letelier, R., Hebel, D., Tupas, L., Dore, J., Christian, J., Winn, C., 1995. Ecosystem changes in the North Pacific subtropical gyre attributed to the 1991-92 El Niño. Nature 373, 230–234. https://doi.org/10.1038/373230a0

Karl, D., Leteller, R., Tupas, L., Dore, J., Christian, J., Hebel, D., 1997. The role of nitrogen fixation in biogeochemical cycling in the subtropical North Pacific Ocean. Nature 388, 533–538. https://doi.org/10.1038/41474

Karl, D.M., 1999. Minireviews: A Sea of Change: Biogeochemical Variability in the North Pacific Subtropical Gyre. Ecosystems 2, 181–214. https://doi.org/10.1007/s100219900068

623 Karl, D.M., Bidigare, R.R., Letelier, R.M., 2001. Long-term changes in plankton community
624 structure and productivity in the North Pacific Subtropical Gyre: The domain shift
625 hypothesis. Deep Sea Res. Part II Top. Stud. Oceanogr. 48, 1449–1470.
626 https://doi.org/10.1016/S0967-0645(00)00149-1
627 Karl, D.M., Church, M.J., Dore, J.E., Letelier, R.M., Mahaffey, C., 2011. Predictable and
628 efficient carbon sequestration in the North Pacific Ocean supported by symbiotic nitrogen
629 fixation. PNAS 109, 6, 1842-1849. https://doi.org/10.1073/pnas.1120312109
630 Laws, E.A., Popp, B.N., Bidigare, R.R., Kennicutt, M.C., Macko, S.A., 1995. Dependence of
631 phytoplankton carbon isotopic composition on growth rate and [CO_2]aq: theoretical
632 considerations and experimental results. Geochim. Cosmochim. Acta 59, 1131–1138.
633 https://doi.org/10.1016/0016-7037(95)00030-4
634 Lee, K.E., Slowey, N.C., Herbert, T.D., 2001. Glacial sea surface temperatures in the subtropical
635 North Pacific: A comparison of Uk_{37}', $\delta^{18}O$, and foraminiferal assemblage temperature
636 estimates. Paleoceanography 16, 268–279. https://doi.org/10.1029/1999PA000493
637 Lu, Z., Liu, Z., Zhu, J., Cobb, K.M., 2018. A review of paleo El Niño-Southern Oscillation.
638 Atmosphere 9, 4, 130. https://doi.org/10.3390/atmos9040130
639 Martin, J.H., Knauer, G.A., Karl, D.M., Broenkow, W.W., 1987. VERTEX: carbon cycling in
640 the northeast Pacific. Deep Sea Res. Part A, Oceanogr. Res. Pap. 34, 267–285.
641 https://doi.org/10.1016/0198-0149(87)90086-0
642 Massana, R., Logares, R., 2013. Eukaryotic versus prokaryotic marine picoplankton ecology.
643 Environ. Microbiol. 15, 5, 1254-1261. https://doi.org/10.1111/1462-2920.12043
644 McMahon, K.M, McCarthy, M., Sherwood, O., Larsen, T., Guilderson, T., 2015. Millennial-
645 scale plankton regime shifts in the subtropical North Pacific Ocean. Science 350, 1530–

1533. https://doi.org/10.1126/science.aaa9942

McMahon, K.M., Williams, B., Guilderson, T. P., Glynn, D.S., and McCarthy, M.D., 2017. Calibrating amino acid $\delta^{13}C$ and $\delta^{15}N$ offsets between polyp and protein skeleton to develop deep-sea proteinaceous corals as paleoceanographic archives. Geochimica et Cosmochimica, 220, 261-27. https://doi.org/10.1016/j.gca.2017.09.048

Monnin, E., Steig, E.J., Siegenthaler, U., Kawamura, K., Schwander, J., Stauffer, B., Stocker, T.F., Morse, D.L., Barnola, J.M., Bellier, B., Raynaud, D., Fischer, H., 2004. Evidence for substantial accumulation rate variability in Antarctica during the Holocene, through synchronization of CO_2 in the Taylor Dome, Dome C and DML ice cores. Earth and Planetary Science Letters, 224 (1-2), 45-54. https://doi.org/10.1016/j.epsl.2004.05.007

Moy, C.M., Seltzer, G.O., Rodbell, D.T., Anderson, D.M., 2002. Variability of El Niño Southern Oscillation activity at millennial timescales during the Holocene epoch. Nature 420, 162–165. https://doi.org/10.1038/nature01194

Pei, Q., Zhang, D.D., Li, J., Lee, H.F., 2017. Proxy-based Northern Hemisphere temperature reconstruction for the Mid-to-Late Holocene. Theor. Appl. Climatol. 130, 1043–1053. https://doi.org/10.1007/s00704-016-1932-5

Polovina, J.J., Howell, E. a., Abecassis, M., 2008. Ocean's least productive waters are expanding. Geophys. Res. Lett. 35, 2–6. https://doi.org/10.1029/2007GL031745

Popp, B.N., Laws, E. a., Bidigare, R.R., Dore, J.E., Hanson, K.L., Wakeham, S.G., 1998. Effect of Phytoplankton Cell Geometry on Carbon Isotopic Fractionation. Geochim. Cosmochim. Acta 62, 69–77. https://doi.org/10.1016/S0016-7037(97)00333-5

Quay, P., Stutsman, J., 2003. Surface layer carbon budget for the subtropical N. Pacific: $\delta^{13}C$ constraints at station ALOHA. Deep. Res. Part I Oceanogr. Res. Pap. 50, 1045–1061.

https://doi.org/10.1016/S0967-0637(03)00116-X

Rau, G.H., Takahashi, T., Des Marais, D.J., 1989. Latitudinal variations in plankton $\delta^{13}C$: implications for CO_2 and productivity in past oceans. Nature 341, 516–518. https://doi.org/10.1038/341516a0

Rau, G.H., Riebesell, U., Wolf-Gladrow, D., 1996. A model of photosynthetic ^{13}C fractionation by marine phytoplankton based on diffusive molecular CO_2 uptake. Mar. Ecol. Prog. Ser. 133, 275–285. https://doi.org/10.3354/meps133275

Reimer, P.J., Bard, E., Bayliss, A., Beck, J.W., Blackwell, P.G., Ramsey, C.B., Buck, C.E., Cheng, H., Edwards, R.L., Friedrich, M., Grootes, P.M., Guilderson, T.P., Haflidason, H., Hajdas, I., Hatté, C., Heaton, T.J., Hoffmann, D.L., Hogg, A.G., Hughen, K.A., Kaiser, K.F., Kromer, B., Manning, S.W., Niu, M., Reimer, R.W., Richards, D.A., Scott, E.M., Southon, J.R., Staff, R.A., Turney, C.S.M., van der Plicht, J., 2013. IntCal13 and Marine13 Radiocarbon Age Calibration Curves 0–50,000 Years cal BP. Radiocarbon 55, 1869–1887. https://doi.org/10.2458/azu_js_rc.55.16947

Roark, E.B., Guilderson, T.P., Dunbar, R.B., Fallon, S.J., Mucciarone, D. A., 2009. Extreme longevity in proteinaceous deep-sea corals. Proc. Natl. Acad. Sci. U. S. A. 106, 5204–5208. https://doi.org/10.1073/pnas.0810875106

Rodionov, S.N., 2004. A sequential algorithm for testing climate regime shifts. Geophys. Res. Lett. 31. https://doi.org/10.1029/2004GL019448. Regime shift program available at: https://www.beringclimate.noaa.gov/regimes/

Schiff, J.T., Batista, F.C., Sherwood, O.A., Guilderson, T.P., Hill, T.M., Ravelo, A.C., McMahon, K.W., Mccarthy, M.D., 2014. Compound specific amino acid $\delta^{13}C$ patterns in a deep-sea proteinaceous coral: Implications for reconstructing detailed $\delta^{13}C$ records of

exported primary production. Mar. Chem. 166, 82–91. https://doi.org/10.1016/j.marchem.2014.09.008

Schneider, T., Bischoff, T., Haug, G.H., 2014. Migrations and dynamics of the intertropical convergence zone. Nature 513, 45–53. https://doi.org/10.1038/nature13636

Scott, K.M., Henn-Sax, M., Harmer, T.L., Longo, D.L., Frame, C.H., Cavanaugh, C.M., 2007. Kinetic isotope effect and biochemical characterization of form IA RubisCO from the marine cyanobacterium Prochlorococcus marinus MIT9313. Limnol. Oceanogr. 52, 2199–2204. https://doi.org/10.4319/lo.2007.52.5.2199

Sherwood, O. A., Scott, D.B., Risk, M.J., 2006. Late Holocene radiocarbon and aspartic acid racemization dating of deep-sea octocorals. Geochim. Cosmochim. Acta 70, 2806–2814. https://doi.org/10.1016/j.gca.2006.03.011

Sherwood, O. A., Guilderson, T.P., Batista, F.C., Schiff, J.T., McCarthy, M.D., 2014. Increasing subtropical North Pacific Ocean nitrogen fixation since the Little Ice Age. Nature 505, 78–81. https://doi.org/10.1038/nature12784

Sigman, D.M., DiFiore, P.J., Hain, M.P., Deutsch, C., Karl, D.M., Bo, V., 2009. Sinking organic matter spreads the nitrogen isotope signal of pelagic denitrification in the North Pacific. Geophysical Research Letters 36, L08605, 1-5. https://doi.org/10.1029/2008GL035784

Tesdal, J.E., Galbraith, E.D., Kienast, M., 2013. Nitrogen isotopes in bulk marine sediment: Linking seafloor observations with subseafloor records. Biogeosciences 10, 101–118. https://doi.org/10.5194/bg-10-101-2013

Young, J.N., Bruggeman, J., Rickaby, R.E.M., Erez, J., Conte, M., 2013. Evidence for changes in carbon isotopic fractionation by phytoplankton between 1960 and 2010. Global Biogeochem. Cycles 27, 505–515. https://doi.org/10.1002/gbc.20045

715 Zubkov, M. V., 2014. Faster growth of the major prokaryotic versus eukaryotic CO_2 fixers in the
716 oligotrophic ocean. Nat. Commun. 5, 1–6. https://doi.org/10.1038/ncomms4776

Figure 1. Study Location. A) SeaWIFS ocean color globe of chlorophyll during boreal summer with Hawai'ian Islands squared in red. **B)** An annual SST (°C) map of Hawaii using World Ocean Atlas 1955-2015 annual data, with arrows pointing to the two coral collection locations on the eastern side of Oahu Island; L for Lanikai (this study), M for Makapu'u (Sherwood et al., 2014), and two sediment core locations P17 and P20 from Lee et al. 2001. Also shown is Station ALOHA from the HOTS program (open circle).

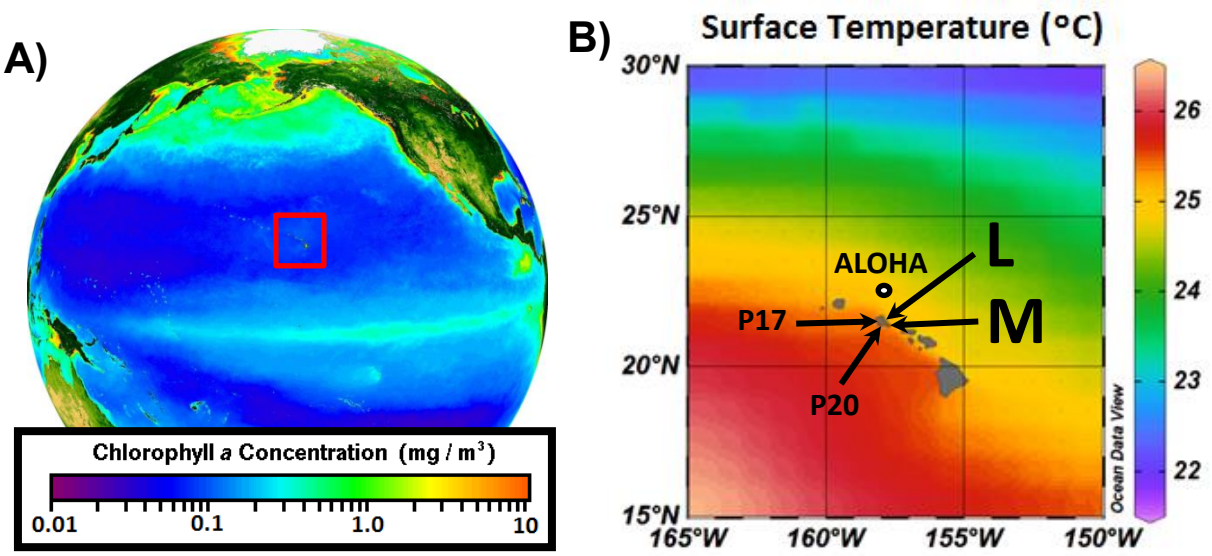

Figure 2. Late Holocene bulk coral $\delta^{15}N$ records compared with selected climactic and sedimentary $\delta^{15}N$ records. **A)** Three new bulk coral $\delta^{15}N$ records from Lanikai (colors indicate coral; *see legend*); blue shading indicates previously published records (Makapu'u) from the same region. **B)** Mid-month insolation 15°N for July which is primarily driven by changes in solar precession cycles (Berger and Loutre, 1991). Also shaded are major ENSO periods where most proxy records agree (Lu et al. 2018). **C)** Data from bulk $\delta^{15}N$ sediment records from the North East Pacific binned by 250 yr time steps from 3 records from offshore Mexico (22 to 23°N), 5 off Central America (7 to 16°N), and 4 in the Eastern Tropical Pacific (ETP, 0 to 1°N). Data from the NICOPP database from Tesdal et al. 2013; see supplemental file for more information. Error bars indicate standard deviation.

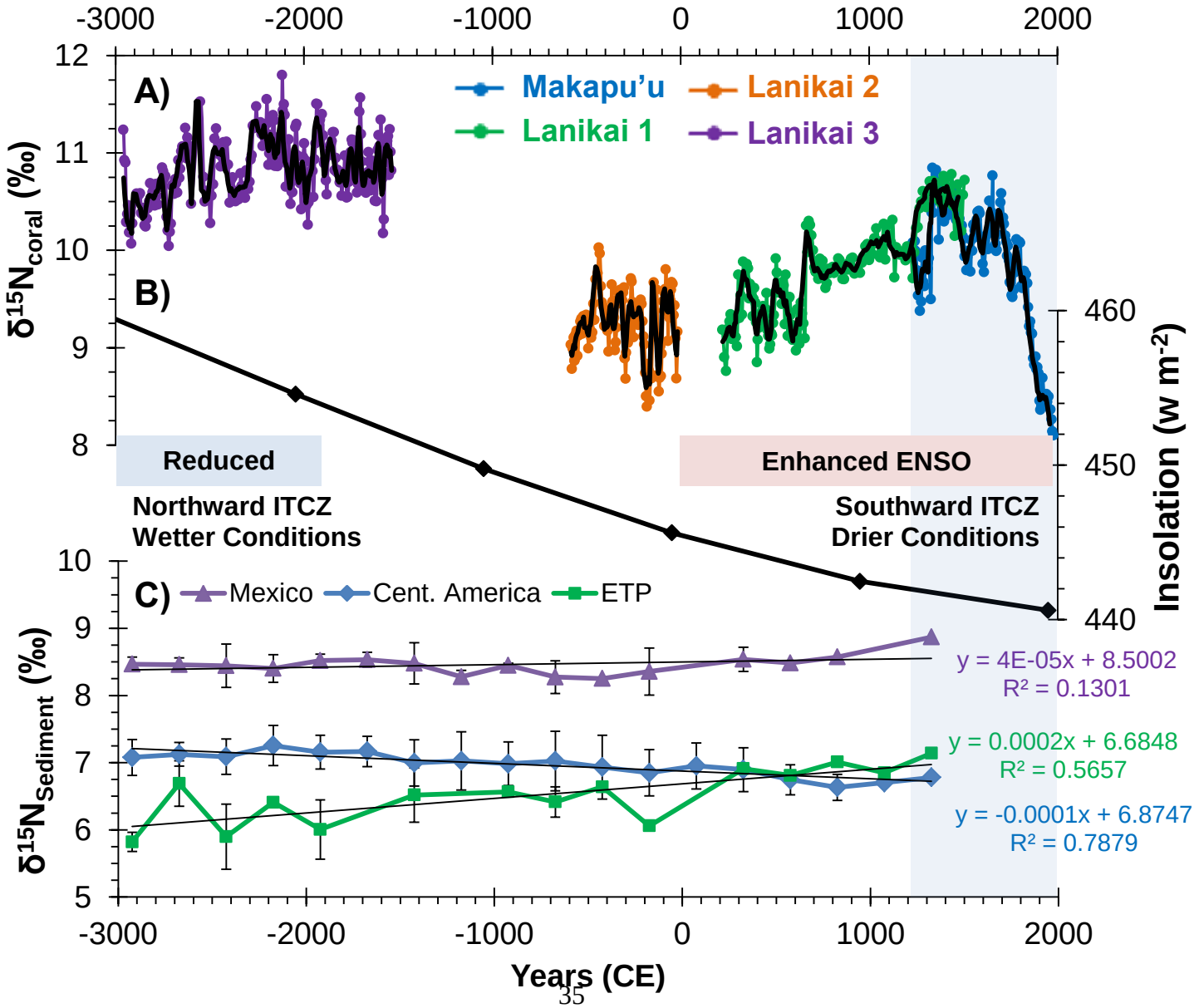

Figure 3. Late Holocene bulk coral $\delta^{13}C$ records compared with selected climactic data, sedimentary and atmospheric $\delta^{13}C$ records. A) Bulk coral carbon isotope record, with blue shading depicting extent of previous coral records from the region, black lines representing a 5 point moving average. **B)** Alkenone SST records for the 2 sediment cores (P17, P20) collected near Oahu, Hawaii (Lee et al. 2001) believed to be representative of wintertime SST conditions in the NPSG. **C)** Atmospheric CO_2 concentration from Antarctic ice core records (Monnin et al. 2004). **D)** Red sediment color intensity record (grey), interpreted to be driven by El Nino Southern Oscillation with the black line designating a 20 year moving average (Moy et al. 2003).

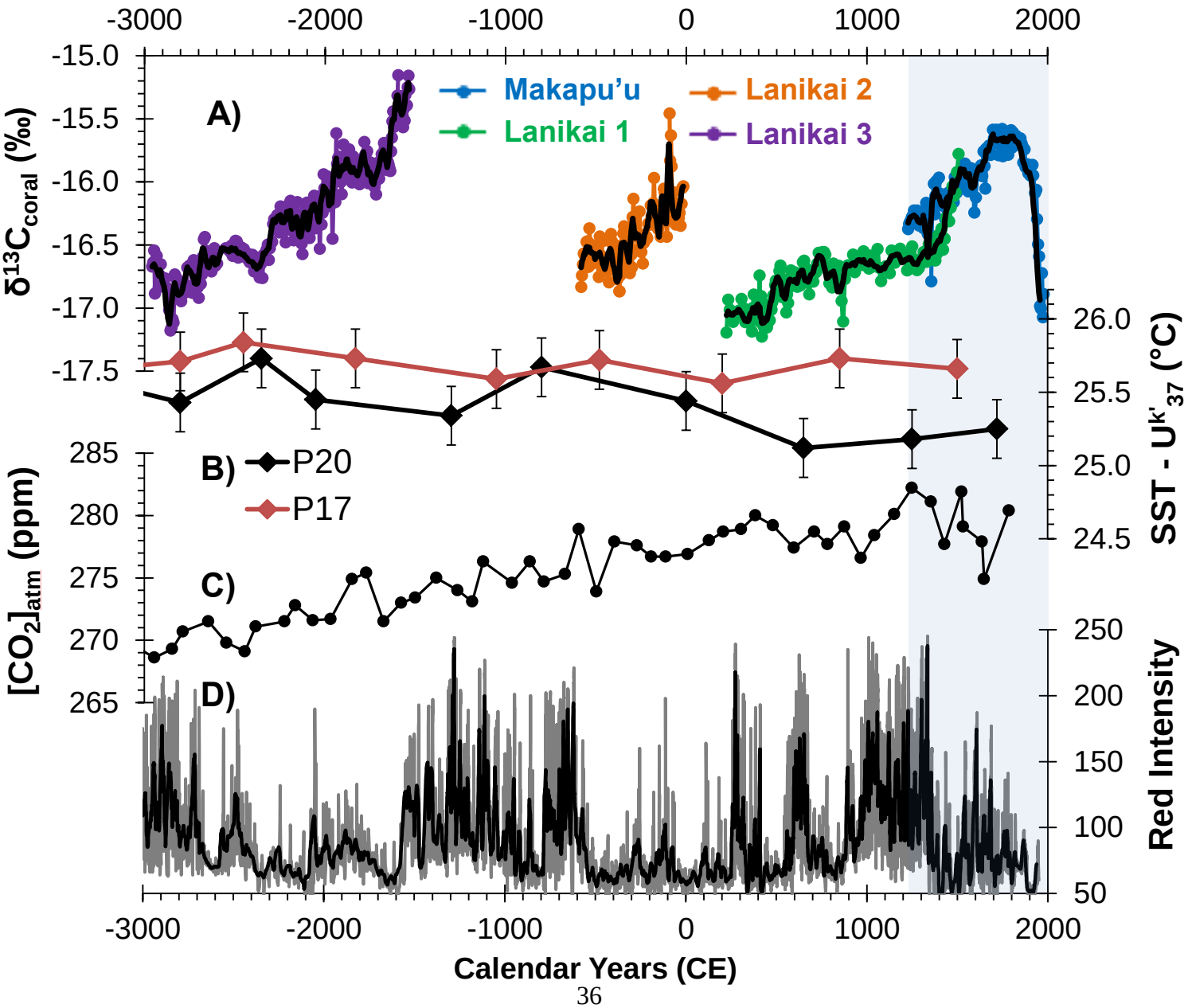

Figure 4. Coupled vs. decoupled changes in $\delta^{15}N$ and $\delta^{13}C$ bulk isotope values of export production in NPSG through the Late-Holocene. Bulk nitrogen and carbon isotopic records from *K. haumeaae* (A and B; as presented in prior figures) are overlain to indicate distinct periods of coupling vs. decoupling in isotopic change. Unshaded periods indicates where $\delta^{15}N$ and $\delta^{13}C$ are decoupled (DC1, DC2), while red shading indicates coupling as the isotope systems trend in the same direction (C1, C2, C3). Grey dashed arrows indicate the assumed trend in isotope values during discontinuities in our current records while black lines designate the 5 point moving average.

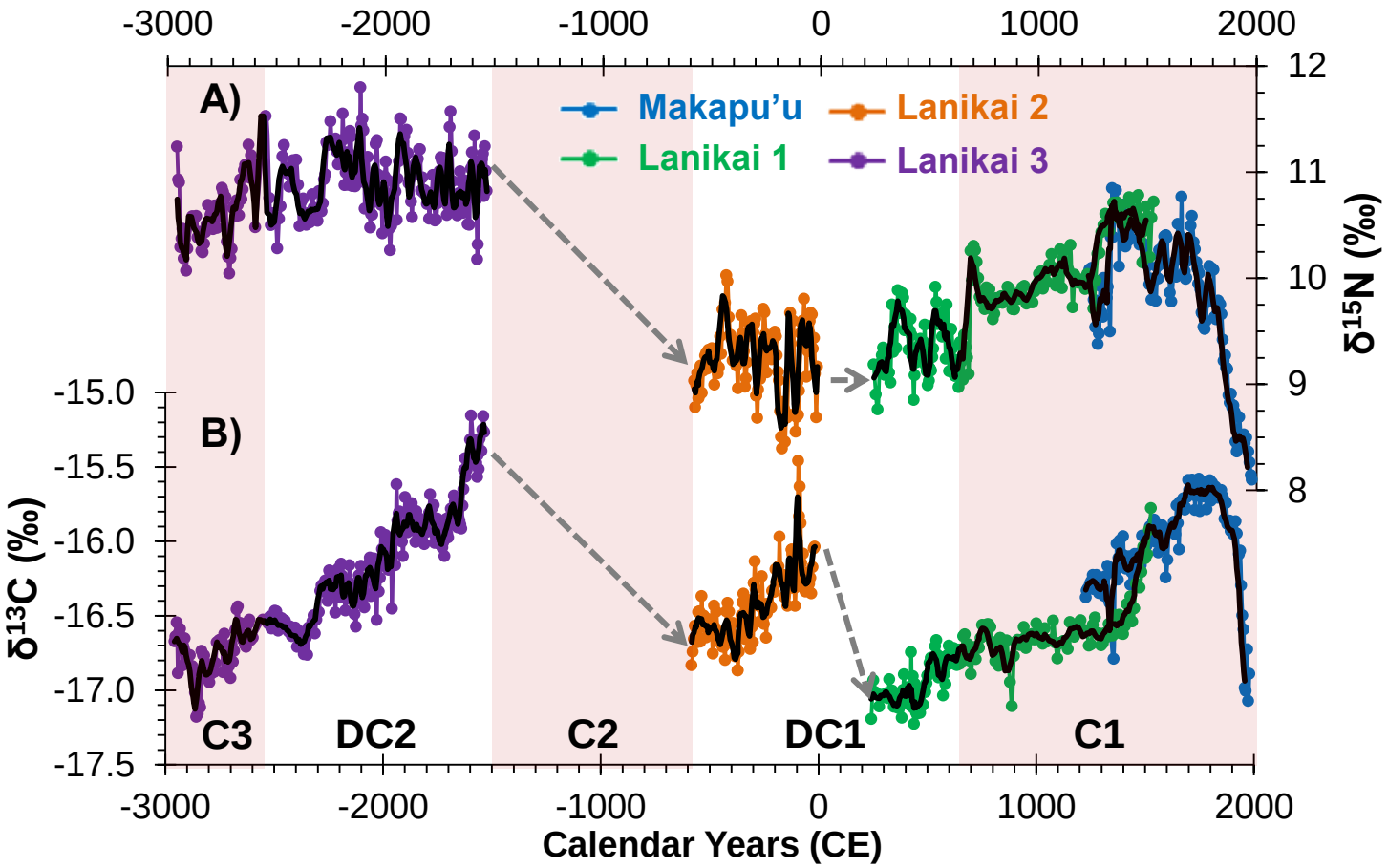

Figure S1. Radiocarbon age models. Age-models were determined for each specimen using a Bayesian modeling approach, Bacon (Blaauw and Christensen 2011) using Marine13 (Reimer et al., 2013) and a reservoir age correction (expressed as ΔR) of -28 ± 4 (Druffel et al., 2001). Blue-shaded areas represent the conventional calibrated ^{14}C age distributions. Dark grey lines represent all iterations (n=10,000) of the model, while the fine red line is based on the weighted mean age for each depth which was used in this study. Lanikai 1 age model was calculated using an accumulation rate of 10 yrs/0.1 mm while Lanikai 2 and 3 used an accumulation rate of 5 yrs/0.1 mm. All corals used an accumulation shape of 1.5, memory strength 4, and a mean memory of 0.7. The grey stippled lines show the 95% confidence intervals which averaged 98 ±15 years. The shape of the curves reflects variable growth rates in the four coral samples illustrated. **A, B, C)** Lanikai corals used in this study with original collection names also listed.

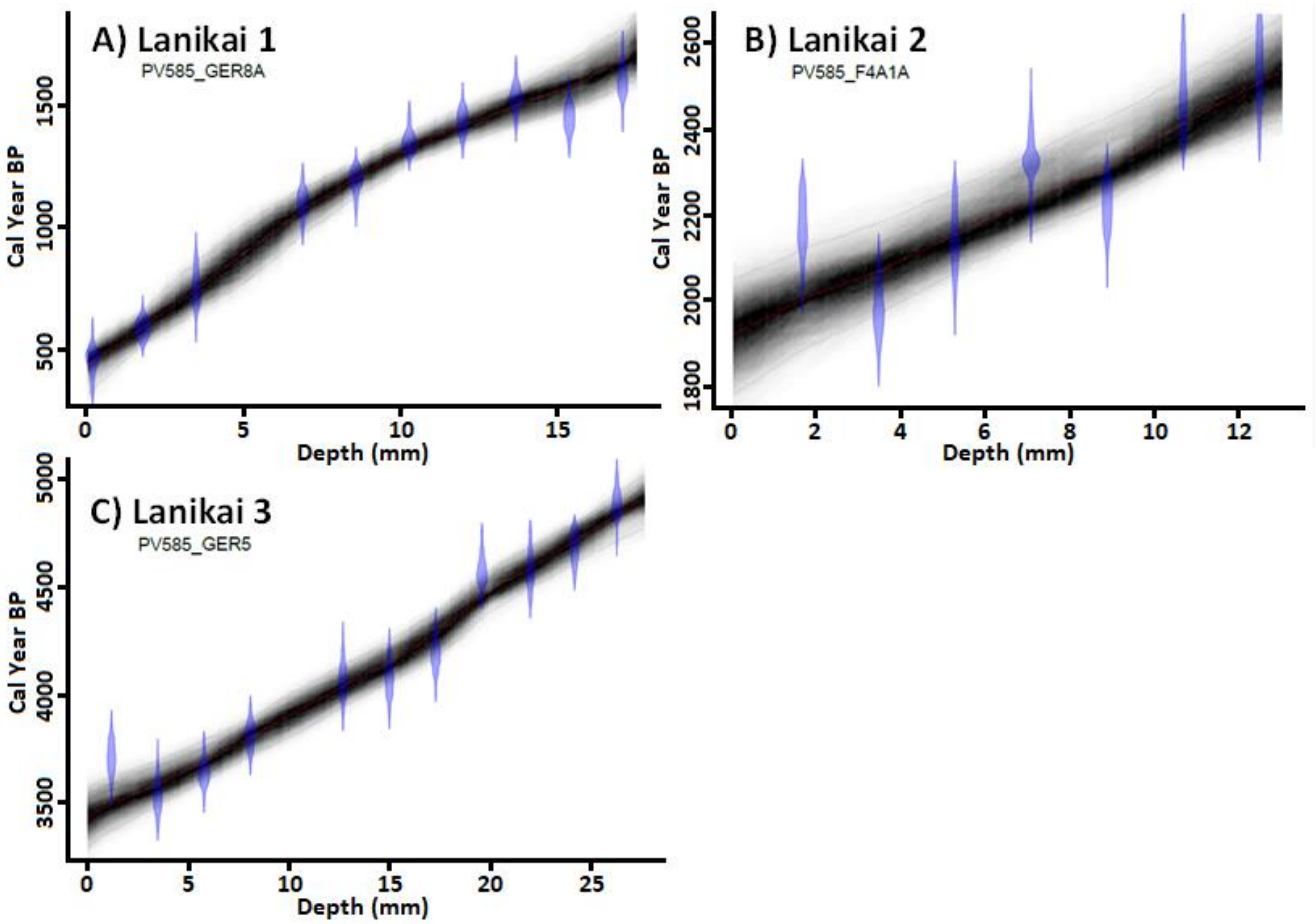

Figure S2. Regime shift detection. A&D) Bulk coral $\delta^{15}N$ and $\delta^{13}C$ records from Lanikai (colors same as previous figures). Black lines signify regimes detected by software designed to automatically detect statistically significant shifts in the mean level and the magnitude of fluctuations in time series using sequential t-tests (Rodionov 2004). **B&E)** $\delta^{15}N$ and $\delta^{13}C$ residuals after the stepwise regime function is removed. **C&F)** Weight attributed to outliers (using Huber's weight function, weight = min(1, parameter/(|anomaly|)), where the anomaly is the deviation from the expected mean value of the new regime normalized by the standard deviation averaged for all consecutive sections of the cut-off length in the series (http://www.beringclimate.noaa.gov/regimes/help.html). If anomalies are less than or equal to the value of the parameter then their weights are equal to one. Otherwise, the weights are inversely proportional to the distance from the expected mean value of the new regime.

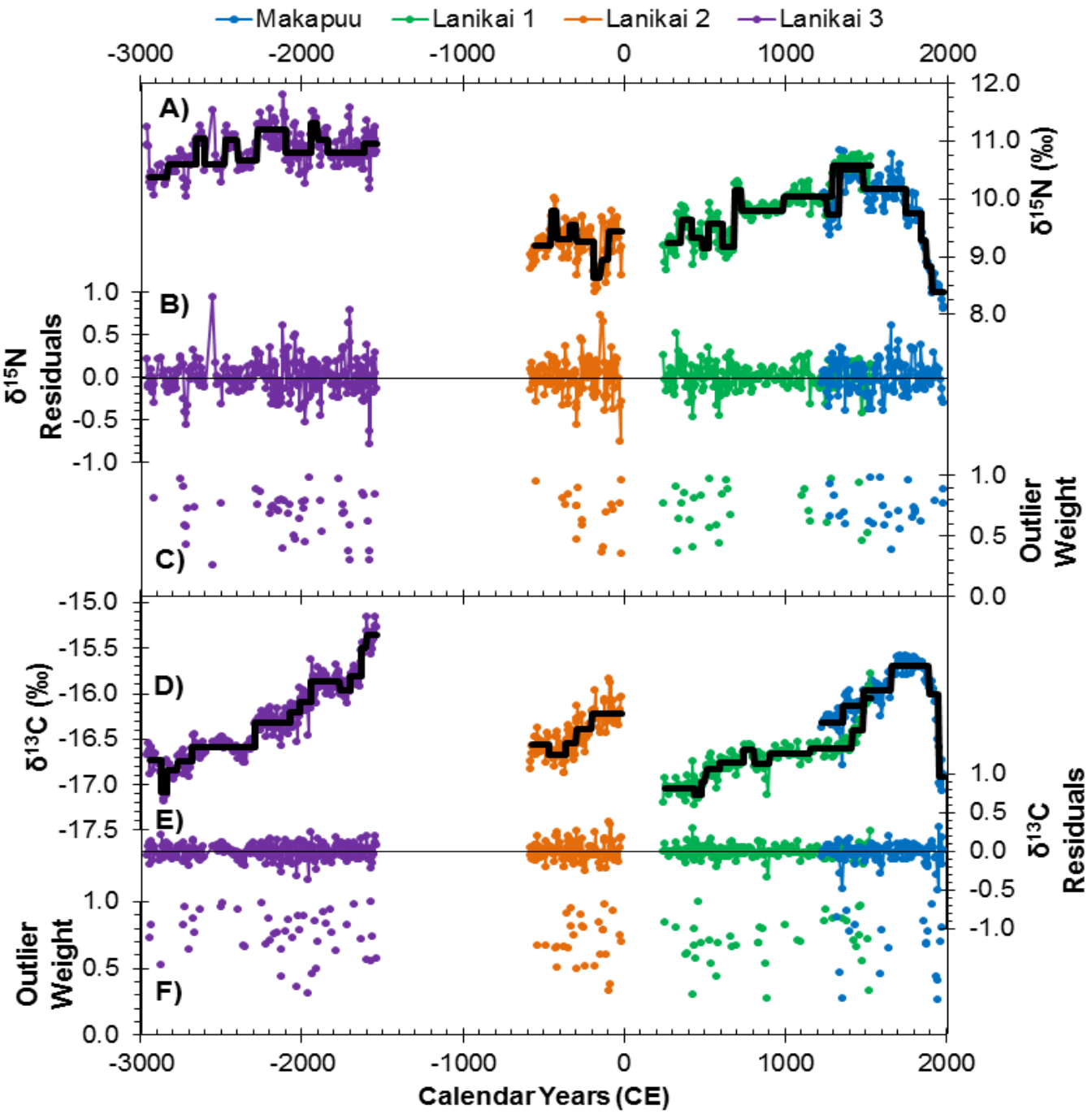
Makapuu
Lanikai 1
Lanikai 2
Lanikai 3
A)
B)
C)
D)
E)
F)
δ15N (‰)
δ15N Residuals
Outlier Weight
δ13C (‰)
δ13C Residuals
Outlier Weight
Calendar Years (CE)

Figure S3. Map of sediment core locations and regional sections. West Pacific (yellow) includes seven sediment $\delta^{15}N$ records published in Kienast et al. (2008), Jia and Li (2011), Langton et al. (2008)*, Rafter and Charles (2012). North West Pacific (red) includes four records published in Kao et al. (2008)*, Kienast (2000). North East Pacific (blue) includes nine records published in Hendy et al (2004)*, McKay et al (2004)*, Chang et al. (2008)*, Emmer and Thunell (2000)*, Kienast et al. (2002), Ganeshram et al. (1995*, 2000*), Arellano-Torres (2010)*. East Pacific (green) includes ten records published in Dubois et al. (2011), Pichevin et al. (2009, 2010), Thunell and Kepple (2004)*, Hendy and Pedersen (2006)*, and Robinson et al. (2009). References marked with a * indicates records using updated age-models. Sedimentary age models were updated using the CALIB program (Stuiver et al. 2017) and Marine13 (Reimer et al., 2013), while retaining reservoir age corrections from the original studies before using a piecewise linear regression to form an updated age model.

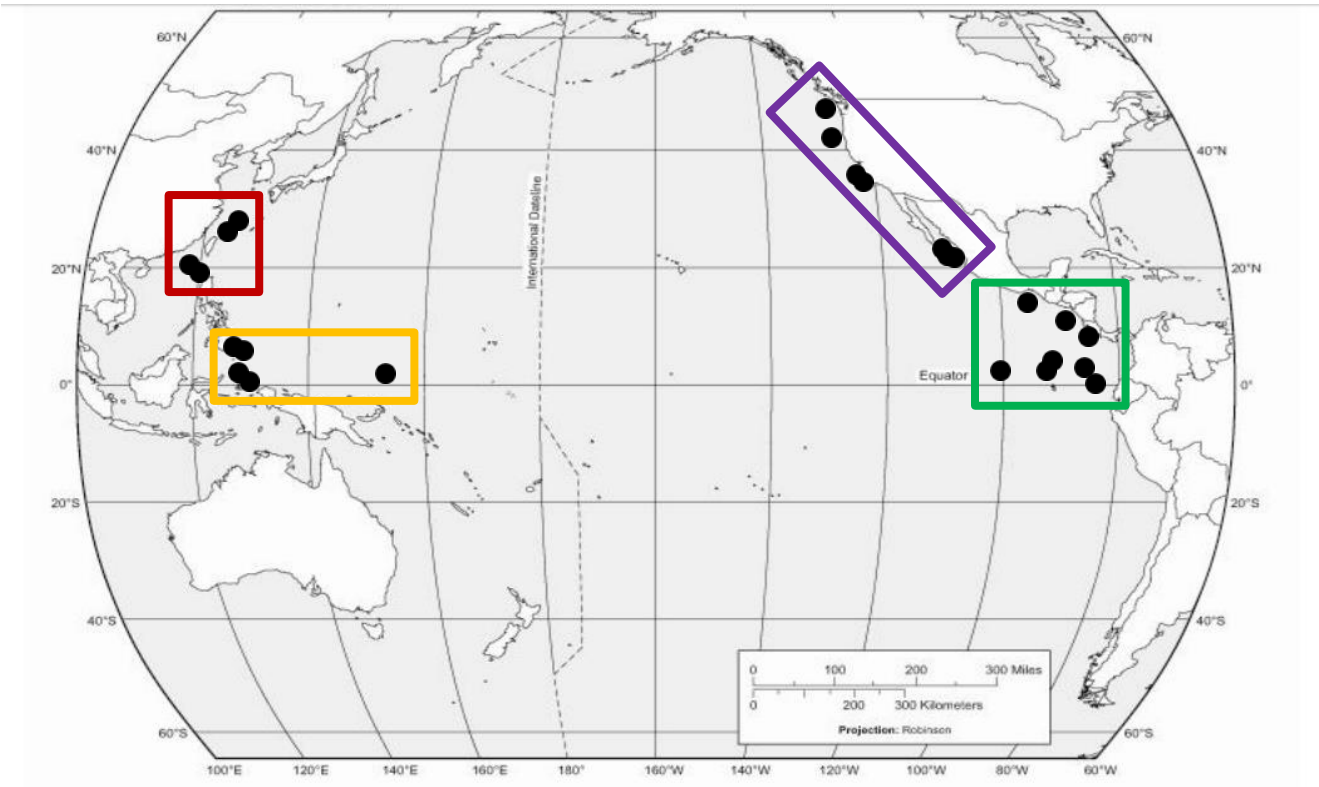

Figure S4. Linear regressions of sedimentary and coral $\delta^{15}N$ records. Sediment data limited to the last 6000 years (-4000 to 2000 CE) and records with >2 points within this period (n=30; see methods). Regions correspond to Fig. S3. Data was standardized to a mean of zero for the 6000 years in order to remove site specific variability in absolute values (e.g. depth differences). Black line designates the overall linear trend of North Pacific sediment $\delta^{15}N$ over 6000 years.

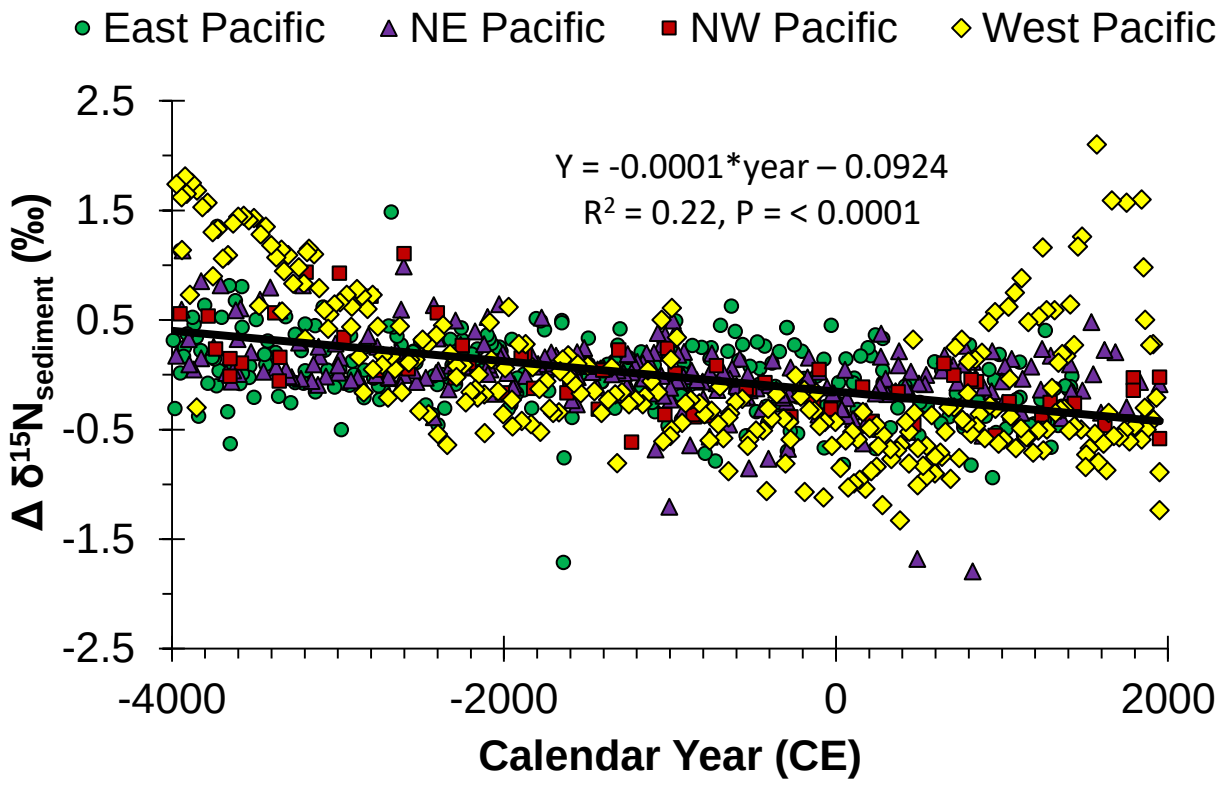

Supplemental Data Table 1 | *K. haumeaae* radiocarbon data. All analysis performed at Lawrence Livermore National Laboratory, following previously established radiocarbon methods for proteinaceous deep-sea corals (Roark et al., 2009, Guilderson et al. 2013). Briefly, this involves converting acid-pretreated coral samples to CO_2 via sealed tube combustion before being reduced to graphite in the presence of an iron catalyst and hydrogen gas (Vogel et al., 1987). Results are reported as Fraction Modern, including both a background and $\delta^{13}C$ correction (cf. Reimer et al., 2004), and as conventional radiocarbon years as per Stuiver and Polach, 1977. A constant ΔR of -28±4 (Druffel et al., 2001) was used for age modeling.

Coral	CAMS ID	ID #	Distance (mm)	$\delta^{13}C$ (‰)	Fraction Modern	error	^{14}C age	error	Model Age (yr BP)	95% Confidence interval	Model Age (yr CE)
Lanikai 1	166951	2	0.2	-15.92	0.9046	0.0055	805	50	451	97	1499
	166952	18	1.8	-16.49	0.8859	0.0040	975	40	589	69	1361
(PV585	166953	35	3.5	-16.60	0.8647	0.0066	1170	70	747	100	1203
Ger8)	166955	69	6.9	-16.77	0.8278	0.0032	1520	35	1072	90	878
	166956	86	8.6	-16.60	0.8191	0.0035	1605	35	1203	72	747
	166957	103	10.3	-16.73	0.8006	0.0028	1785	30	1325	59	625
	166958	120	12	-16.92	0.7932	0.0028	1860	30	1419	69	531
	166959	137	13.7	-17.15	0.7846	0.0027	1950	30	1503	79	447
	166960	154	15.4	-17.00	0.7918	0.0031	1875	35	1582	98	368
	166961	171	17.1	-17.11	0.7793	0.0037	2005	40	1691	123	259
Lanikai 2	166962	17	1.7	-16.22	0.7347	0.0031	2475	35	2001	117	-51
	166963	35	3.5	-16.09	0.7488	0.0028	2325	35	2069	106	-119
(PV585	166964	53	5.3	-16.34	0.7370	0.0033	2450	40	2152	97	-202
F4A1)	166965	71	7.1	-16.32	0.7220	0.0024	2615	30	2239	93	-289
	166966	89	8.9	-16.64	0.7304	0.0031	2525	35	2312	96	-362
	166967	107	10.7	-16.63	0.7122	0.0028	2725	35	2413	94	-463
	166968	125	12.5	-16.68	0.7090	0.0033	2765	40	2507	112	-557
Lanikai 3	168323	12	1.2	-15.16	0.6276	0.0034	3740	45	3489	124	-1539
	168324	35	3.5	-15.65	0.6392	0.0036	3595	50	3581	104	-1631
(PV585	168325	58	5.8	-16.03	0.6322	0.0023	3685	30	3682	94	-1732
GER5)	168326	81	8.1	-16.01	0.6212	0.0023	3825	30	3801	89	-1851
	168327	127	12.7	-16.45	0.6068	0.0031	4015	45	4036	96	-2086
	168328	150	15	-16.38	0.6067	0.0029	4015	40	4147	97	-2197
	168329	173	17.3	-16.59	0.6005	0.0024	4095	35	4280	102	-2330
	168330	196	19.6	-16.58	0.5798	0.0021	4380	30	4455	100	-2505
	168331	220	22	-16.67	0.5796	0.0029	4380	45	4589	96	-2639
	168332	242	24.2	-16.68	0.5739	0.0022	4460	35	4713	95	-2763
	168333	263	26.3	-16.77	0.5621	0.0029	4630	45	4837	109	-2887

Supplemental Data Table 2 | *K. haumeaae* $\delta^{13}C$ and $\delta^{15}N$ bulk data and C:N ratios. All analysis performed at the Stable Isotope Lab of the University of California Santa Cruz using VPDB and N_2 air as standards for $\delta^{13}C$ and $\delta^{15}N$ respectively. Any samples with an identification ending in "D" are duplicate analyses. Samples with a * symbol in ID were excluded from analysis due to an abnormal C:N ratio (below 2.7 or above 3.1) and/or an estimated mass of under 20 μg N (which approaches the limit of detection for $\delta^{15}N$ on an EA-IRMS).

ID	depth (mm)	Year (CE)	95% CI (yrs)	$\delta^{13}C$ (‰)	$\delta^{15}N$ (‰)	C:N Ratio	ID	depth (mm)	Year (CE)	95% CI (yrs)	$\delta^{13}C$ (‰)	$\delta^{15}N$ (‰)	C:N Ratio
L1_1	0.1	1508	101	-15.78	10.72	3.07	**L3_1***	0.1	-1483	139	-15.88	11.85	3.62
L1_2	0.2	1499	97	-15.92	10.57	3.03	**L3_2***	0.2	-1489	137	-15.13	12.19	3.26
L1_3	0.3	1490	93	-16.09	10.20	3.14	**L3_3***	0.3	-1494	135	-14.94	12.04	3.13
L1_4	0.4	1481	91	-16.12	10.58	3.00	**L3_4***	0.4	-1499	133	-15.05	12.08	3.06
L1_5	0.5	1473	92	-16.04	10.67	2.95	**L3_5***	0.5	-1504	132	-15.15	11.92	3.05
L1_6	0.6	1464	95	-16.21	10.44	3.02	**L3_6***	0.6	-1510	132	-14.86	11.25	3.03
L1_7*	0.7	1456	91	-16.31	10.15	3.11	**L3_6D***	0.6	-1510	132	-16.39	10.57	2.86
L1_8	0.8	1447	87	-16.31	10.46	2.98	**L3_7***	0.7	-1515	130	-14.93	10.97	3.07
L1_9	0.9	1439	84	-16.28	10.78	2.96	**L3_8***	0.8	-1520	128	-15.02	11.22	3.07
L1_10	1.0	1430	85	-16.43	10.56	3.08	**L3_9***	0.9	-1525	127	-15.07	11.10	3.00
L1_10D	1.0	1430	85	-16.47	10.66	2.88	**L3_10***	1.0	-1530	126	-15.13	10.80	3.03
L1_11	1.1	1421	87	-16.54	10.54	3.10	**L3_11**	1.1	-1535	125	-15.27	10.82	3.04
L1_12	1.2	1413	81	-16.37	10.75	2.94	**L3_12**	1.2	-1539	124	-15.16	11.01	3.02
L1_13	1.3	1404	77	-16.53	10.52	3.05	**L3_13**	1.3	-1543	123	-15.25	11.24	2.99
L1_14	1.4	1396	74	-16.42	10.76	2.97	**L3_14**	1.4	-1548	123	-15.40	10.77	3.01
L1_15	1.5	1388	73	-16.57	10.57	3.03	**L3_15**	1.5	-1552	122	-15.40	11.17	2.95
L1_16	1.6	1379	74	-16.62	10.49	3.03	**L3_16**	1.6	-1556	123	-15.31	11.12	3.00
L1_17	1.7	1370	71	-16.62	10.52	3.04	**L3_17**	1.7	-1560	121	-15.52	11.11	3.02
L1_18	1.8	1361	69	-16.49	10.69	3.00	**L3_18**	1.8	-1564	120	-15.42	10.91	2.96
L1_19	1.9	1351	70	-16.53	10.56	3.03	**L3_19**	1.9	-1568	119	-15.57	10.98	2.98
L1_20	2.0	1342	74	-16.50	10.71	2.95	**L3_20**	2.0	-1572	118	-15.48	10.78	2.95
L1_21	2.1	1332	80	-16.63	10.68	3.04	**L3_21**	2.1	-1576	118	-15.36	10.32	2.96
L1_22	2.2	1323	80	-16.59	10.71	2.96	**L3_22**	2.2	-1579	116	-15.35	10.17	2.96
L1_23	2.3	1314	81	-16.56	10.61	2.94	**L3_23**	2.3	-1584	115	-15.45	10.74	2.97
L1_24	2.4	1305	84	-16.64	10.44	2.99	**L3_24**	2.4	-1587	114	-15.32	10.86	2.95
L1_25	2.5	1295	90	-16.68	10.46	3.08	**L3_25**	2.5	-1591	113	-14.76	11.34	2.83
L1_25D	2.5	1295	90	-16.56	10.47	2.88	**L3_26**	2.6	-1595	114	-15.16	10.87	3.00

L1_26	2.6	1287	96	-16.68	10.61	2.93	**L3_27**	2.7	-1599	111	-15.32	11.07	2.98
L1_27	2.7	1278	94	-16.70	10.50	3.02	**L3_28**	2.8	-1603	110	-15.47	11.18	2.98
L1_28	2.8	1268	94	-16.62	10.43	2.97	**L3_29**	2.9	-1607	109	-15.49	11.03	2.94
L1_29	2.9	1259	95	-16.62	10.24	2.97	**L3_30**	3.0	-1611	109	-15.48	10.92	2.97
L1_30	3.0	1250	99	-16.51	10.23	2.91	**L3_31**	3.1	-1615	109	-15.52	10.50	3.03
L1_31	3.1	1241	103	-16.56	9.98	2.94	**L3_32**	3.2	-1619	107	-15.57	10.83	2.98
L1_32	3.2	1232	100	-16.69	9.71	3.08	**L3_33**	3.3	-1623	106	-15.44	10.51	3.00
L1_33	3.3	1222	98	-16.70	9.97	2.96	**L3_34**	3.4	-1627	105	-15.52	10.85	2.94
L1_34	3.4	1213	98	-16.61	9.93	2.98	**L3_35**	3.5	-1631	104	-15.65	10.80	2.96
L1_35	3.5	1203	100	-16.60	10.04	2.94	**L3_36**	3.6	-1635	104	-15.76	10.83	2.98
L1_36	3.6	1194	104	-16.59	9.90	2.94	**L3_37**	3.6	-1640	103	-15.92	10.92	2.94
L1_37	3.7	1184	102	-16.53	9.95	2.95	**L3_38**	3.8	-1644	102	-15.89	10.61	2.96
L1_38	3.8	1174	102	-16.55	9.99	2.94	**L3_39**	3.9	-1648	101	-15.86	10.64	2.93
L1_39	3.9	1165	104	-16.58	9.95	2.90	**L3_40**	4.0	-1653	102	-15.84	10.91	2.91
L1_40	4.0	1155	107	-16.64	9.98	2.93	**L3_41**	4.1	-1657	102	-15.91	11.01	2.95
L1_41	4.1	1145	113	-16.62	10.03	2.92	**L3_42**	4.2	-1661	101	-15.73	10.80	2.94
L1_42	4.2	1136	111	-16.54	9.72	2.96	**L3_43**	4.3	-1666	100	-15.79	10.67	2.96
L1_43	4.3	1126	110	-16.73	10.31	2.95	**L3_44**	4.4	-1670	100	-15.74	10.59	2.96
L1_44	4.4	1116	112	-16.69	10.08	3.01	**L3_45**	4.5	-1674	100	-15.69	10.65	2.97
L1_45	4.5	1106	115	-16.70	10.29	2.92	**L3_46**	4.6	-1679	100	-15.80	10.71	2.94
L1_45D	4.5	1106	115	-16.65	10.00	2.85	**L3_47**	4.7	-1683	99	-15.84	10.71	2.96
L1_46	4.6	1097	120	-16.68	10.26	2.88	**L3_48**	4.8	-1687	98	-15.78	10.67	2.95
L1_47	4.7	1088	117	-16.69	9.91	2.91	**L3_49**	4.9	-1692	97	-15.89	10.91	2.96
L1_48	4.8	1078	115	-16.79	10.27	2.97	**L3_50**	5.0	-1696	98	-15.84	11.19	2.93
L1_49	4.9	1068	116	-16.68	9.99	3.01	**L3_51**	5.1	-1701	98	-15.98	11.57	2.97
L1_50	5.0	1058	118	-16.53	9.93	2.92	**L3_52**	5.2	-1705	97	-15.87	11.40	2.96
L1_51	5.1	1049	121	-16.66	10.09	2.94	**L3_52D**	5.2	-1705	97	-16.02	11.44	2.94
L1_52	5.2	1039	118	-16.67	10.23	2.91	**L3_53**	5.3	-1709	96	-15.85	10.70	2.97
L1_53	5.3	1030	116	-16.68	10.12	2.88	**L3_54**	5.4	-1714	95	-15.92	10.68	2.92
L1_54	5.4	1020	116	-16.59	9.96	2.94	**L3_55**	5.4	-1718	96	-16.10	10.59	2.96
L1_55	5.5	1010	117	-16.69	10.05	2.89	**L3_56**	5.6	-1722	97	-16.01	10.71	2.97
L1_56	5.6	1000	120	-16.63	9.90	2.88	**L3_57**	5.7	-1727	95	-16.04	10.82	2.93
L1_57	5.7	991	115	-16.63	10.06	2.93	**L3_58**	5.8	-1732	94	-16.03	10.85	2.94
L1_58	5.8	981	112	-16.55	10.04	2.91	**L3_59**	5.9	-1736	94	-15.89	11.13	2.94
L1_59	5.9	972	111	-16.66	9.94	2.93	**L3_60**	6.0	-1741	94	-16.02	11.10	2.94
L1_60	6.0	962	111	-16.62	9.87	2.91	**L3_61**	6.1	-1746	95	-15.86	11.14	2.94
L1_61	6.1	953	112	-16.63	9.77	2.96	**L3_62**	6.2	-1751	94	-15.85	11.01	2.95
L1_62	6.2	943	107	-16.67	9.77	2.99	**L3_63**	6.3	-1756	93	-15.97	10.78	2.94
L1_63	6.3	933	103	-16.72	9.80	2.98	**L3_64**	6.4	-1762	92	-16.01	10.70	2.92
L1_64	6.4	924	101	-16.58	9.76	2.96	**L3_65**	6.5	-1767	92	-15.76	10.55	2.93

L1_65	6.5	914	100	-16.66	9.92	2.93	**L3_66**	6.6	-1773	94	-15.77	10.54	2.92
L1_66	6.6	904	101	-16.70	9.91	2.92	**L3_67**	6.7	-1778	92	-15.79	10.76	2.97
L1_67	6.7	896	96	-16.66	9.87	2.94	**L3_68**	6.8	-1783	91	-15.69	10.97	2.91
L1_68	6.8	887	92	-16.68	9.80	2.94	**L3_69**	6.9	-1788	90	-15.75	10.75	2.97
L1_69	6.9	878	90	-16.77	9.85	2.88	**L3_69D**	6.9	-1788	90	-15.87	10.86	2.95
L1_70	7.0	869	90	-17.11	9.70	3.05	**L3_70**	7.0	-1794	91	-15.86	10.74	2.93
L1_71	7.1	860	92	-16.95	9.70	2.98	**L3_71**	7.1	-1799	92	-15.94	10.56	2.93
L1_72	7.2	852	89	-16.83	9.81	2.97	**L3_72**	7.2	-1804	91	-15.92	10.72	2.94
L1_73	7.3	845	87	-16.67	9.90	2.87	**L3_73**	7.3	-1810	90	-16.02	10.70	2.95
L1_74	7.4	837	86	-16.79	9.92	2.90	**L3_74**	7.3	-1815	90	-15.89	10.78	2.91
L1_75	7.5	830	88	-16.78	9.83	2.90	**L3_75**	7.5	-1820	90	-15.99	10.83	2.89
L1_76	7.6	823	90	-16.67	9.83	2.84	**L3_76**	7.6	-1825	91	-15.89	10.80	2.91
L1_77	7.7	815	86	-16.71	9.77	2.86	**L3_77**	7.7	-1831	89	-15.85	10.95	2.91
L1_77D	7.7	815	86	-16.59	9.77	2.83	**L3_78**	7.8	-1836	88	-15.94	10.82	2.89
L1_78	7.8	807	83	-16.84	9.83	2.88	**L3_79**	7.9	-1841	87	-15.95	11.21	2.94
L1_79	7.9	800	81	-16.80	9.78	2.85	**L3_80**	8.0	-1846	88	-15.80	11.21	2.90
L1_80	8.0	792	81	-16.81	9.76	2.85	**L3_81**	8.1	-1851	89	-16.01	11.12	2.93
L1_81	8.1	785	83	-16.70	9.81	2.86	**L3_82**	8.2	-1857	88	-15.92	11.09	2.91
L1_82	8.2	777	77	-16.68	9.66	2.88	**L3_83**	8.3	-1862	88	-15.87	11.07	2.87
L1_83	8.3	770	74	-16.58	9.61	2.86	**L3_84**	8.4	-1867	88	-15.75	10.97	2.88
L1_84	8.4	762	72	-16.56	9.72	2.83	**L3_85**	8.5	-1872	89	-15.77	11.00	2.91
L1_85	8.5	755	71	-16.56	9.89	2.86	**L3_86**	8.6	-1878	91	-15.80	10.57	2.89
L1_86	8.6	747	72	-16.60	9.72	2.86	**L3_87**	8.7	-1883	91	-15.87	10.82	2.88
L1_87	8.7	740	69	-16.64	9.91	2.83	**L3_87D**	8.7	-1883	91	-15.97	10.62	2.88
L1_88	8.8	732	68	-16.56	9.70	2.86	**L3_88**	8.8	-1888	91	-15.94	10.93	2.89
L1_89	8.9	725	68	-16.65	9.86	2.88	**L3_89**	8.9	-1893	91	-15.90	10.89	2.88
L1_90	9.0	717	70	-16.66	9.84	2.86	**L3_90**	9.0	-1898	93	-15.70	11.18	2.86
L1_90D	9.0	717	70	-16.77	9.71	2.93	**L3_91**	9.1	-1903	95	-15.90	11.40	2.90
L1_91	9.1	710	74	-16.71	9.82	2.87	**L3_92**	9.1	-1908	94	-16.10	11.16	2.93
L1_92	9.2	703	71	-16.79	10.00	2.84	**L3_93**	9.3	-1913	94	-16.00	11.34	2.94
L1_93	9.3	695	69	-16.71	10.15	2.81	**L3_94**	9.4	-1918	95	-15.97	11.28	2.89
L1_94	9.4	688	69	-16.76	10.26	2.81	**L3_95**	9.5	-1923	96	-15.80	11.18	2.89
L1_95	9.5	681	70	-16.89	10.30	2.84	**L3_96**	9.6	-1928	98	-15.81	11.50	3.04
L1_96	9.6	674	73	-16.80	9.98	2.86	**L3_97**	9.7	-1933	97	-15.86	11.50	2.90
L1_97	9.7	667	68	-16.69	10.26	2.85	**L3_98**	9.8	-1938	96	-15.62	11.10	3.01
L1_98	9.8	659	65	-16.76	9.10	2.84	**L3_99**	9.9	-1944	97	-16.16	10.94	3.00
L1_99	9.9	652	63	-16.63	9.25	2.78	**L3_100**	10.0	-1949	98	-16.00	10.55	3.01
L1_100	10.0	645	63	-16.64	9.35	2.78	**L3_101**	10.1	-1954	100	-16.09	10.81	3.04
L1_101	10.1	638	65	-16.80	9.46	2.78	**L3_102**	10.2	-1959	99	-16.45	10.82	2.97
L1_102	10.2	632	61	-16.82	9.04	2.81	**L3_103**	10.3	-1964	99	-16.14	10.90	2.92

L1_103	10.3	625	59	-16.73	9.21	2.79	**L3_104**	10.4	-1969	99	-16.01	10.77	2.92
L1_104	10.4	619	59	-16.83	9.39	2.81	**L3_105**	10.5	-1974	100	-16.19	10.49	3.03
L1_105	10.5	613	60	-16.83	8.97	2.83	**L3_106**	10.6	-1979	101	-16.15	10.26	2.98
L1_106	10.6	606	63	-16.76	9.08	2.87	**L3_107**	10.7	-1984	100	-15.93	10.48	3.02
L1_107	10.7	601	62	-16.72	9.12	2.83	**L3_107D**	10.7	-1984	100	-16.15	10.45	2.95
L1_108	10.8	596	62	-16.71	9.24	2.78	**L3_108**	10.8	-1989	99	-15.96	10.77	2.98
L1_108D	10.8	596	62	-16.89	8.92	2.81	**L3_109**	10.9	-1994	99	-16.17	10.93	2.92
L1_109	10.9	590	63	-16.82	9.23	2.83	**L3_110**	11.0	-1999	100	-16.06	11.10	2.99
L1_110	11.0	585	65	-16.77	9.34	2.78	**L3_111**	11.1	-2004	101	-16.05	10.96	2.90
L1_111	11.1	579	68	-16.70	9.52	2.77	**L3_112**	11.2	-2009	100	-15.94	10.78	2.84
L1_112	11.2	574	67	-16.77	9.51	2.80	**L3_113**	11.3	-2014	98	-16.25	10.42	2.96
L1_113	11.3	569	66	-16.84	9.12	2.97	**L3_114**	11.4	-2019	98	-16.34	10.69	2.89
L1_114	11.4	564	66	-16.96	9.52	2.78	**L3_115**	11.5	-2024	99	-16.24	10.74	2.89
L1_115	11.5	558	68	-16.89	9.75	2.81	**L3_116**	11.6	-2029	100	-16.53	10.85	2.94
L1_116	11.6	553	70	-17.04	9.24	-	**L3_117**	11.7	-2035	98	-16.23	10.97	2.91
L1_117	11.7	548	68	-16.91	9.64	2.74	**L3_118**	11.8	-2040	97	-16.12	11.30	2.85
L1_118	11.8	542	67	-16.78	9.68	2.79	**L3_119**	11.9	-2045	98	-16.13	11.26	2.83
L1_119	11.9	537	67	-16.85	9.45	2.88	**L3_120**	12.0	-2050	98	-16.15	10.95	2.91
L1_120	12.0	531	69	-16.92	9.63	2.81	**L3_121**	12.1	-2055	99	-16.37	10.72	2.94
L1_121	12.1	526	71	-16.76	9.57	2.85	**L3_122**	12.2	-2060	98	-16.11	10.59	2.92
L1_122	12.2	521	70	-16.67	9.64	2.82	**L3_123**	12.3	-2065	96	-16.15	10.60	2.85
L1_123	12.3	516	70	-16.71	9.56	2.81	**L3_124**	12.4	-2071	96	-16.16	10.48	2.85
L1_124	12.4	511	71	-16.79	9.77	2.80	**L3_125**	12.5	-2076	96	-16.36	10.79	2.90
L1_125	12.5	506	73	-16.85	9.92	2.78	**L3_126**	12.6	-2081	97	-16.36	11.14	2.80
L1_126	12.6	501	75	-16.79	9.56	2.80	**L3_127**	12.6	-2086	96	-16.45	10.88	2.96
L1_127	12.7	496	74	-16.78	9.33	2.79	**L3_128**	12.8	-2091	95	-16.43	10.96	2.87
L1_128	12.8	491	74	-16.82	9.25	2.85	**L3_129**	12.9	-2096	95	-16.32	10.47	2.97
L1_129*	12.9	486	75	-17.79	9.13	3.21	**L3_129D**	12.9	-2096	95	-16.27	10.84	2.93
L1_130	13.0	481	76	-16.91	9.07	2.80	**L3_130**	13.0	-2101	96	-16.17	11.39	2.89
L1_130D	13.0	481	76	-16.90	9.22	2.86	**L3_131**	13.1	-2106	97	-16.24	11.50	2.84
L1_131	13.1	476	78	-16.95	9.03	2.84	**L3_132**	13.2	-2111	96	-16.23	11.44	2.84
L1_132	13.2	471	77	-17.01	8.99	2.82	**L3_133**	13.3	-2116	95	-16.29	11.80	2.85
L1_133	13.3	466	76	-16.98	9.12	2.84	**L3_134**	13.4	-2120	95	-16.42	10.96	2.93
L1_134	13.4	461	77	-17.10	9.18	2.86	**L3_135**	13.5	-2125	96	-16.57	10.90	2.94
L1_135	13.5	457	78	-17.10	9.56	2.84	**L3_136**	13.6	-2130	97	-16.49	11.15	2.88
L1_136	13.6	452	80	-17.11	9.40	2.86	**L3_137**	13.7	-2135	96	-16.39	11.15	2.82
L1_137	13.7	447	79	-17.15	9.33	2.85	**L3_138**	13.8	-2139	96	-16.29	10.86	2.88
L1_138	13.8	442	80	-17.03	9.41	2.80	**L3_139**	13.9	-2144	96	-16.35	10.90	2.83
L1_139	13.9	437	81	-17.11	9.43	2.73	**L3_140**	14.0	-2149	96	-16.31	10.99	2.88
L1_140	14.0	432	83	-17.16	9.37	2.87	**L3_141**	14.1	-2154	97	-16.16	10.87	2.90

L1_141	14.1	428	85	-17.14	9.34	2.85	**L3_142**	14.2	-2159	96	-16.27	11.33	2.84
L1_142	14.2	423	85	-16.96	9.24	2.87	**L3_143**	14.3	-2163	95	-16.34	11.39	2.84
L1_143	14.3	419	86	-17.23	9.20	2.79	**L3_144**	14.4	-2168	96	-16.39	11.18	2.91
L1_144	14.4	414	87	-16.91	9.33	2.88	**L3_145**	14.5	-2173	96	-16.47	10.88	2.93
L1_145	14.5	410	89	-17.11	9.08	2.81	**L3_146***	14.6	-2178	97	-17.10	11.18	3.10
L1_146	14.6	405	92	-16.74	8.85	2.94	**L3_147**	14.7	-2183	96	-16.29	10.99	2.86
L1_147	14.7	401	91	-17.10	9.26	2.86	**L3_148**	14.8	-2188	96	-16.25	11.04	2.84
L1_148	14.8	396	92	-16.98	9.46	2.84	**L3_148D**	14.8	-2188	96	-16.21	10.72	2.94
L1_149	14.9	392	93	-17.08	9.61	2.81	**L3_149**	14.9	-2192	96	-16.15	11.31	2.83
L1_150	15.0	387	95	-17.02	9.39	2.71	**L3_150**	15.0	-2197	97	-16.38	11.55	2.79
L1_150D	15.0	387	95	-17.00	9.61	2.88	**L3_151**	15.1	-2202	98	-16.18	11.19	2.87
L1_151	15.1	383	97	-17.04	9.32	2.88	**L3_152**	15.2	-2207	97	-16.28	11.16	2.85
L1_152	15.2	378	96	-17.05	9.52	2.88	**L3_153**	15.3	-2213	97	-16.20	11.21	2.85
L1_153	15.3	373	96	-16.89	9.63	2.89	**L3_154**	15.4	-2218	97	-16.48	11.07	2.84
L1_154	15.4	368	98	-17.00	9.65	2.85	**L3_155**	15.5	-2224	98	-16.31	11.19	2.78
L1_155	15.5	364	99	-17.19	9.51	2.89	**L3_156**	15.6	-2229	100	-16.35	11.31	2.84
L1_156	15.6	359	102	-17.06	9.82	2.77	**L3_157**	15.7	-2235	98	-16.24	11.29	2.88
L1_157	15.7	352	102	-17.12	9.86	2.81	**L3_158**	15.8	-2241	99	-16.22	11.27	2.88
L1_158	15.8	346	103	-17.12	9.70	2.75	**L3_159**	15.9	-2247	99	-16.20	11.30	2.87
L1_159	15.9	339	105	-17.05	9.67	2.80	**L3_160**	16.0	-2253	101	-16.40	11.48	2.90
L1_160	16.0	333	108	-17.11	9.88	2.87	**L3_161**	16.1	-2259	103	-16.30	11.29	2.82
L1_161	16.1	326	112	-17.11	9.34	2.86	**L3_162**	16.2	-2265	102	-16.26	11.25	2.79
L1_162	16.2	319	111	-17.00	9.54	2.79	**L3_163**	16.3	-2271	101	-16.29	11.28	2.79
L1_163	16.3	313	112	-17.06	9.30	2.86	**L3_164**	16.4	-2277	101	-16.34	10.98	2.87
L1_164	16.4	306	113	-16.93	9.75	2.75	**L3_165**	16.5	-2282	102	-16.30	10.93	2.91
L1_165	16.5	299	116	-17.06	9.02	2.93	**L3_166**	16.6	-2288	104	-16.34	10.70	2.84
L1_166	16.6	292	119	-17.11	9.06	2.91	**L3_167**	16.7	-2294	103	-16.55	10.61	2.88
L1_166D	16.6	292	119	-16.93	9.15	2.91	**L3_167D**	16.7	-2294	103	-16.41	10.65	2.91
L1_167	16.7	286	118	-17.04	9.26	2.83	**L3_168***	16.8	-2300	102	-14.79	11.70	2.80
L1_168	16.8	279	118	-17.04	9.10	2.82	**L3_169**	16.9	-2306	102	-16.53	10.82	2.88
L1_169	16.9	272	118	-17.05	9.09	2.82	**L3_170**	17.0	-2312	103	-16.62	10.54	2.83
L1_170	17.0	266	120	-17.03	9.34	2.81	**L3_171**	17.1	-2318	105	-16.50	10.64	2.88
L1_171	17.1	259	123	-17.11	9.27	2.74	**L3_172**	17.2	-2324	103	-16.54	10.59	2.84
L1_172	17.2	250	123	-17.03	9.19	2.78	**L3_173**	17.3	-2330	102	-16.59	10.66	2.89
L1_173	17.3	241	126	-17.01	8.76	2.88	**L3_174**	17.4	-2336	102	-16.61	10.79	2.84
L1_174	17.4	232	131	-16.93	8.90	2.81	**L3_175**	17.5	-2342	103	-16.58	10.57	2.89
L1_175	17.5	222	137	-17.20	9.18	2.82	**L3_176**	17.6	-2348	104	-16.76	10.52	2.83
							L3_177	17.7	-2355	102	-16.65	10.61	2.85
L2_1*	0.1	27	135	-16.32	9.85	3.53	**L3_178**	17.8	-2363	102	-16.76	10.50	2.92
L2_2*	0.2	22	133	-17.01	9.18	3.80	**L3_179**	17.9	-2371	103	-16.62	10.60	2.84

L2_3*	0.3	18	132	-15.72	9.01	3.32	**L3_180**	18.0	-2378	105	-16.65	10.75	2.89
L2_4*	0.4	13	131	-15.53	9.32	3.17	**L3_181**	18.1	-2386	108	-16.60	10.72	2.84
L2_5*	0.5	8	131	-15.65	9.54	3.02	**L3_182**	18.2	-2394	106	-16.71	10.49	2.90
L2_6*	0.6	3	130	-15.79	8.94	3.23	**L3_183**	18.3	-2402	105	-16.58	10.88	2.87
L2_7*	0.7	-2	128	-15.94	8.97	3.16	**L3_184**	18.4	-2410	105	-16.62	11.11	2.84
L2_8*	0.8	-7	126	-15.60	8.84	3.06	**L3_185**	18.5	-2418	107	-16.64	10.89	2.92
L2_9*	0.9	-12	125	-15.94	8.86	3.10	**L3_186**	18.6	-2426	109	-16.63	11.09	2.94
L2_10	1.0	-17	123	-16.04	9.16	3.04	**L3_186D**	18.6	-2426	109	-16.52	11.12	2.89
L2_11*	1.1	-22	123	-16.05	8.68	3.13	**L3_187**	18.7	-2434	106	-16.61	10.96	2.93
L2_12*	1.2	-27	121	-16.18	9.10	3.19	**L3_188**	18.8	-2442	104	-16.59	10.86	2.90
L2_13	1.3	-32	119	-16.35	9.43	3.05	**L3_189**	18.9	-2450	103	-16.53	10.99	2.90
L2_14	1.4	-37	118	-16.25	9.33	3.07	**L3_190**	19.0	-2458	104	-16.58	11.03	2.90
L2_15	1.5	-42	118	-16.29	9.66	3.00	**L3_191**	19.1	-2466	107	-16.52	11.25	2.89
L2_16	1.6	-47	118	-16.29	9.67	3.01	**L3_192**	19.2	-2474	103	-16.58	11.15	2.90
L2_17	1.7	-51	117	-16.22	9.59	2.93	**L3_193**	19.3	-2481	99	-16.60	10.68	2.92
L2_18	1.8	-55	116	-16.36	9.41	3.00	**L3_194**	19.4	-2489	99	-16.47	10.56	2.91
L2_18D	1.8	-55	116	-16.22	9.56	2.90	**L3_195**	19.5	-2497	99	-16.47	10.28	2.93
L2_19	1.9	-59	115	-16.34	9.31	3.01	**L3_196**	19.6	-2505	100	-16.58	10.57	2.92
L2_20	2.0	-63	115	-16.23	9.47	2.92	**L3_197**	19.7	-2512	97	-16.59	10.56	2.89
L2_21	2.1	-67	115	-16.21	9.07	3.08	**L3_198**	19.8	-2519	96	-16.51	10.61	2.89
L2_22	2.2	-71	114	-16.08	9.51	2.94	**L3_199**	19.9	-2526	95	-16.55	10.50	2.90
L2_23	2.3	-75	113	-16.26	9.55	3.02	**L3_200**	20.0	-2533	96	-16.54	10.75	2.89
L2_24	2.4	-78	112	-16.15	9.80	2.92	**L3_201**	20.1	-2540	98	-	-	-
L2_25	2.5	-82	112	-15.88	9.60	2.96	**L3_202**	20.2	-2545	97	-	-	-
L2_26	2.6	-86	112	-15.63	9.56	3.02	**L3_203**	20.3	-2551	96	-16.53	11.53	2.88
L2_27	2.7	-89	110	-15.83	9.38	3.02	**L3_204**	20.4	-2556	97	-	-	-
L2_28*	2.8	-93	109	-15.46	9.48	3.03	**L3_205**	20.5	-2561	98	-	-	-
L2_29	2.9	-97	109	-	-	-	**L3_206**	20.6	-2567	99	-	-	-
L2_30	3.0	-100	109	-16.26	8.94	2.99	**L3_207**	20.7	-2572	98	-	-	-
L2_31	3.1	-104	108	-16.31	8.71	2.98	**L3_208**	20.8	-2577	97	-	-	-
L2_32	3.2	-108	107	-16.44	9.01	2.93	**L3_209**	20.9	-2582	97	-	-	-
L2_33	3.3	-112	106	-16.32	8.69	2.92	**L3_210**	21.0	-2587	97	-	-	-
L2_34	3.4	-115	106	-16.32	8.55	3.00	**L3_211**	21.1	-2592	98	-	-	-
L2_35	3.5	-119	106	-16.09	8.72	2.85	**L3_212**	21.2	-2598	97	-16.65	10.48	2.92
L2_36	3.6	-123	105	-16.05	9.00	2.91	**L3_213**	21.3	-2603	96	-	10.92	-
L2_36D	3.6	-123	105	-16.06	9.22	2.84	**L3_214**	21.4	-2608	96	-16.67	11.07	2.90
L2_37	3.7	-128	104	-16.24	9.60	2.90	**L3_215**	21.5	-2613	97	-16.53	11.02	2.89
L2_38	3.8	-132	103	-	-	-	**L3_216**	21.6	-2619	98	-16.55	11.16	2.89
L2_39	3.9	-137	102	-	-	-	**L3_217**	21.7	-2624	96	-16.65	10.94	2.96
L2_40	4.0	-142	103	-16.44	9.67	2.88	**L3_218**	21.8	-2629	96	-16.71	11.26	2.96

L2_41	4.1	-146	103	-	-	-	**L3_219**	21.9	-2634	96	-16.69	11.05	2.96
L2_42	4.2	-151	102	-	-	-	**L3_220**	22.0	-2639	96	-16.67	10.98	2.90
L2_43	4.3	-156	101	-16.38	8.68	2.85	**L3_221**	22.1	-2644	98	-16.66	11.07	2.94
L2_44	4.4	-160	101	-16.23	8.73	2.86	**L3_222**	22.2	-2650	96	-16.62	11.02	2.92
L2_45	4.5	-165	101	-16.28	8.46	3.01	**L3_223**	22.3	-2655	95	-16.55	10.83	2.94
L2_46	4.6	-170	102	-16.24	8.77	2.84	**L3_224**	22.4	-2661	95	-16.58	10.74	2.95
L2_47	4.7	-174	100	-16.23	8.83	2.82	**L3_225**	22.5	-2667	95	-16.44	10.93	2.96
L2_48	4.8	-179	99	-15.97	8.39	2.89	**L3_226**	22.6	-2672	97	-16.46	10.59	2.99
L2_49	4.9	-184	98	-16.17	8.50	2.85	**L3_227**	22.7	-2678	96	-16.57	10.65	2.92
L2_50	5.0	-188	99	-16.18	8.74	2.93	**L3_227D**	22.7	-2678	96	-16.62	10.72	2.91
L2_51	5.1	-193	99	-16.28	9.03	2.88	**L3_228**	22.8	-2683	96	-16.74	10.73	2.90
L2_52	5.2	-198	98	-16.19	9.12	2.87	**L3_229**	22.9	-2689	96	-16.81	10.58	2.92
L2_53	5.3	-202	97	-16.34	9.27	2.86	**L3_230**	23.0	-2695	97	-16.70	10.68	2.95
L2_54	5.4	-207	96	-16.38	9.42	2.88	**L3_231**	23.1	-2700	99	-16.92	10.66	2.92
L2_54D	5.4	-207	96	-16.28	9.48	2.81	**L3_232**	23.2	-2706	98	-16.84	10.27	2.93
L2_55	5.5	-212	97	-16.33	9.49	2.82	**L3_233**	23.3	-2712	97	-16.78	10.19	2.94
L2_56	5.6	-217	97	-16.45	9.26	2.94	**L3_234**	23.4	-2717	97	-16.76	10.04	2.92
L2_57	5.7	-222	96	-16.44	9.41	2.92	**L3_235**	23.5	-2723	98	-16.72	10.20	2.90
L2_58	5.8	-226	95	-16.44	9.23	2.97	**L3_236**	23.6	-2729	99	-16.62	10.34	2.92
L2_59	5.9	-231	95	-16.42	9.39	2.87	**L3_237**	23.7	-2735	97	-16.88	10.76	2.95
L2_60	6.0	-236	96	-16.48	9.40	2.88	**L3_238**	23.8	-2740	95	-16.67	10.73	2.91
L2_61	6.1	-240	97	-16.65	9.26	2.93	**L3_239**	23.9	-2746	95	-16.66	10.81	2.91
L2_62	6.2	-245	95	-16.42	9.41	2.89	**L3_240**	24.0	-2752	95	-16.67	10.85	2.91
L2_63	6.3	-250	95	-16.56	9.11	2.87	**L3_241**	24.1	-2758	96	-16.73	10.77	2.91
L2_64	6.4	-255	94	-16.44	9.47	2.83	**L3_241D**	24.1	-2758	96	-16.65	10.64	3.04
L2_65	6.5	-260	94	-16.24	9.68	2.87	**L3_242**	24.2	-2763	95	-16.68	10.65	2.92
L2_66	6.6	-264	95	-16.44	9.71	2.85	**L3_243**	24.3	-2769	93	-16.82	10.65	2.93
L2_67	6.7	-269	93	-16.54	9.14	3.00	**L3_244**	24.4	-2774	93	-16.88	10.47	2.94
L2_68	6.8	-274	93	-16.41	9.17	2.84	**L3_245**	24.5	-2780	93	-16.87	10.56	2.93
L2_69	6.9	-279	92	-16.40	9.05	2.88	**L3_246**	24.6	-2785	94	-16.83	10.68	2.91
L2_70	7.0	-284	92	-16.43	9.14	2.89	**L3_247**	24.7	-2792	93	-16.90	10.46	2.92
L2_71	7.1	-289	93	-16.32	8.95	2.86	**L3_248**	24.8	-2797	93	-16.95	10.50	2.91
L2_72	7.2	-293	92	-16.13	8.68	2.86	**L3_249**	24.9	-2803	94	-16.90	10.60	2.88
L2_73	7.3	-297	92	-16.34	8.91	2.90	**L3_250**	25.0	-2809	96	-16.91	10.54	2.93
L2_73D	7.3	-297	92	-16.22	8.87	2.91	**L3_251**	25.1	-2815	98	-16.82	10.69	2.90
L2_74	7.4	-301	93	-16.68	9.62	2.93	**L3_252**	25.2	-2821	98	-16.77	10.50	2.92
L2_75	7.5	-305	94	-16.58	9.57	2.86	**L3_253**	25.3	-2827	99	-16.77	10.43	2.90
L2_76	7.6	-309	96	-16.53	9.49	2.88	**L3_254**	25.4	-2833	100	-16.74	10.32	2.90
L2_77	7.7	-313	95	-16.72	9.58	2.86	**L3_255**	25.5	-2839	102	-17.12	10.24	2.90
L2_78	7.8	-317	95	-16.67	9.57	2.77	**L3_256**	25.6	-2845	105	-17.09	10.26	2.91

L2_79	7.9	-321	95	-16.59	9.59	2.81
L2_80	8.0	-325	96	-16.42	9.47	2.88
L2_81	8.1	-329	97	-16.39	9.50	2.88
L2_82	8.2	-333	96	-16.45	9.57	2.84
L2_83	8.3	-337	96	-16.66	9.45	2.84
L2_84	8.4	-341	97	-16.54	9.20	2.85
L2_85	8.5	-345	97	-16.35	9.05	2.83
L2_86	8.6	-349	97	-16.41	8.97	2.86
L2_87	8.7	-353	97	-16.50	9.31	2.79
L2_88	8.8	-358	96	-16.63	9.44	2.83
L2_89	8.9	-362	96	-16.64	9.47	2.91
L2_90	9.0	-366	96	-16.74	9.65	2.83
L2_91	9.1	-370	97	-16.96	9.69	2.92
L2_91D	9.1	-370	97	-16.77	8.95	2.83
L2_92	9.2	-376	96	-16.71	9.35	2.83
L2_93	9.3	-382	95	-16.77	8.96	2.91
L2_94	9.4	-388	95	-16.70	9.17	2.86
L2_95	9.5	-393	95	-16.55	9.25	2.84
L2_96	9.6	-399	96	-16.67	9.34	2.82
L2_97	9.7	-405	95	-16.60	9.22	2.87
L2_98	9.8	-411	94	-16.47	9.42	2.84
L2_99	9.9	-417	94	-16.41	9.46	2.83
L2_100	10.0	-423	95	-16.47	9.63	2.82
L2_101	10.1	-429	97	-16.80	9.97	2.81
L2_102	10.2	-434	95	-16.71	10.03	2.80
L2_103	10.3	-440	94	-16.71	9.76	2.81
L2_104	10.4	-446	94	-16.62	9.70	2.81
L2_105	10.5	-452	95	-16.62	9.70	2.79
L2_106	10.6	-458	96	-16.68	9.28	2.85
L2_107	10.7	-463	94	-16.63	9.45	2.77
L2_108	10.8	-469	94	-16.48	9.16	2.76
L2_109	10.9	-474	95	-16.58	9.10	2.77
L2_110	11.0	-479	96	-16.43	9.18	2.75
L2_111	11.1	-485	98	-16.76	9.21	2.82
L2_112	11.2	-490	98	-16.63	8.99	2.83
L2_113	11.3	-495	98	-16.54	9.29	2.73
L2_114	11.4	-501	99	-16.52	9.34	2.73
L2_115	11.5	-506	101	-	-	-
L2_116	11.6	-511	104	-	-	-
L2_117	11.7	-516	103	-16.65	9.32	2.81

L3_257	25.7	-2851	105	-17.16	10.43	2.90
L3_258	25.8	-2857	105	-17.10	10.38	2.94
L3_258D	25.8	-2857	105	-17.26	10.36	2.89
L3_259	25.9	-2863	105	-17.02	10.38	2.93
L3_260	26.0	-2869	107	-16.87	10.58	2.93
L3_261	26.1	-2875	109	-16.84	10.57	2.92
L3_262	26.2	-2881	109	-	-	-
L3_263	26.3	-2887	109	-16.77	10.58	2.93
L3_264	26.4	-2893	109	-	-	-
L3_265	26.5	-2899	111	-	-	-
L3_266	26.6	-2905	113	-	-	-
L3_267	26.7	-2910	114	-16.65	10.28	2.91
L3_268	26.8	-2916	114	-16.74	10.07	2.91
L3_269	26.9	-2921	116	-16.84	10.36	2.93
L3_270	27.0	-2927	118	-16.65	10.18	2.93
L3_271	27.1	-2932	120	-16.59	10.46	2.92
L3_272	27.2	-2937	121	-16.70	10.43	2.92
L3_272D	27.2	-2937	121	-16.53	10.31	2.93
L3_273	27.3	-2942	122	-16.89	10.29	3.03
L3_274	27.4	-2947	123	-16.55	10.90	2.92
L3_275	27.5	-2952	125	-16.64	10.93	2.90
L3_276	27.6	-2958	127	-16.67	11.24	2.90

L2_118	11.8	-521	103	-16.52	9.14	2.75
L2_119	11.9	-527	105	-16.50	9.30	2.72
L2_120	12.0	-532	106	-16.57	9.27	2.70
L2_121	12.1	-537	109	-16.37	9.18	2.70
L2_122	12.2	-542	108	-16.68	9.12	2.77
L2_123	12.3	-547	109	-16.47	8.92	2.78
L2_124	12.4	-552	110	-16.48	9.17	2.74
L2_125	12.5	-557	112	-16.68	9.13	2.80
L2_126	12.6	-562	114	-16.39	9.05	2.96
L2_126D	12.6	-562	114	-16.78	8.68	2.79
L2_127	12.7	-567	114	-16.57	9.10	2.74
L2_128	12.8	-572	116	-16.66	8.99	2.83
L2_129	12.9	-578	117	-16.74	8.78	2.79
L2_130	13.0	-583	119	-16.83	9.03	2.84

Supplemental Data Table 3 | Sensitivity of $\delta^{13}C$ according to different environmental variables.

Variable	$\delta^{13}C$ sensitivity	Surface Seasonal Variable Range	Theoretical Seasonal $\Delta\delta^{13}C$	References
Temperature on ε_p	0.12‰ / °C	24-27 °C	0.36‰	Locarnini et al. 2010, Young et al. 2013
Temperature on $\delta^{13}C_{plankton}$	0.11‰ / °C *	24-27 °C	0.33‰	Rau et al. 1996
Temperature on $\delta^{13}C_{plankton}$	0.23‰ / °C	24-27 °C	0.69‰	Rau et al. 1989
Temperature on suspended POC	0.41‰ / °C	24-27 °C	1.23‰	Rau et al. 1992
pH	2.7‰ / 0.1 pH	8.085-8.115 pH	0.08‰	Hinga et al. 1994, Dore et al. 2009
Salinity on ε_p	0.003‰ / PSU	34.5 – 35.3 PSU	0.002‰	Antonov et al. 2010, Young et al. 2013
$\delta^{13}C$ of DIC on ε_p	0.99‰ / ‰	1.25 – 1.45 ‰	0.20‰	Quay et al. 2003, Young et. al. 2013
pCO_2 on ε_p	0.0003‰ / ppm	20 ppm	0.006‰	Takahashi et al. 2009, Young et al. 2013, Keeling et al. 2004
Species fractionation (ε_f)	0.55‰ / ‰ *	23.1-25.6‰ (Range for 0-200m)	1.37‰ (not seasonal value)	Rau et al. 1996, Hernes and Benner 2002 (upper 200m)

* Calculated based off equations and values found in Rau et al. 1996.

Supplemental References:

Antonov, J.I., Seidov, D., Boyer, T.P., Locarnini, R.A., Mishonov, A. V., Garcia, H.E., Baranova, O.K., Zweng, M.M., Johnson, D.R., 2010. World Ocean Atlas 2009, Volume 2: Salinity, NOAA Atlas NESDIS 69. 10.1182/blood-2011-06-357442

Arellano-Torres, E., 2010. Paleoceanography of the https://doi.org/Eastern Tropical North Pacific on Millennial Timescales. Univ. Edinburgh. Dissertation: https://www.era.lib.ed.ac.uk/handle/1842/4634

Blaauw, M., Christen, J.A., 2011. Flexible paleoclimate age-depth models using an autoregressive gamma process. Bayesian Anal. 6, 457–474. https://doi.org/10.1214/11-BA618

Chang, A.S., Pedersen, T.F., Hendy, I.L., 2008. Late Quaternary paleoproductivity history on the Vancouver Island margin, western Canada: a multiproxy geochemical study. Can. J. Earth Sci. 45, 1283–1297. https://doi.org/10.1139/E08-054

Dore, J.E., Lukas, R., Sadler, D.W., Church, M.J., Karl, D.M., 2009. Physical and biogeochemical modulation of ocean acidification in the central North Pacific. Proc. Natl. Acad. Sci. 106, 12235–12240. https://doi.org/10.1073/pnas.0906044106

Druffel, E.R.M., Griffin, S., Guilderson, T.P., Kashgarian, M., Southon, J., Schrag, D.P., 2001. Changes of subtropical North Pacific radiocarbon and correlation with climate variability. Radiocarbon 43(1) 15-25. https://doi.org/10.1017/S0033822200031593

Dubois, N., Kienast, M., Kienast, S., Normandeau, C., Calvert, S.E., Herbert, T.D., Mix, A., 2011. Millennial-scale variations in hydrography and biogeochemistry in the Eastern Equatorial Pacific over the last 100 kyr. Quat. Sci. Rev. 30, 210–223. https://doi.org/10.1016/j.quascirev.2010.10.012

Emmer, E., Thunell, R.C., 2000. Nitrogen isotope variations in Santa Barbara Basin sediments: Implications for denitrification in the eastern tropical North Pacific during the last 50,000 years. Paleoceanography 15, 377–387. https://doi.org/10.1029/1999PA000417

Ganeshram, R.S., Pedersen, T.F., Calvert, S.E., McNeill, G.W., Fontugne, M.R., 2000. Glacial-interglacial variability in denitrification in the world's oceans: Causes and consequences. Paleoceanography 15, 361–376. https://doi.org/10.1029/1999PA000422

Ganeshram, R.S., Pedersen, T.F., Calvert, S.E., Murray, J.W., 1995. Large changes in oceanic nutrient inventories from glacial to interglacial periods. Nature 376, 755–758. https://doi.org/10.1038/376755a0

Guilderson, T.P., McCarthy, M.D., Dunbar, R.B., Englebrecht, a., Roark, E.B., 2013. Late Holocene variations in Pacific surface circulation and biogeochemistry inferred from proteinaceous deep-sea corals. Biogeosciences 10, 6019–6028. https://doi.org/10.5194/bg-10-6019-2013

Hendy, I.L., Pedersen, T.F., 2006. Oxygen minimum zone expansion in the Eastern Tropical North Pacific during deglaciation. Geophys. Res. Lett. 33, 1–5. doi:10.1029/2006GL025975

Hendy, I.L., Pedersen, T.F., Kennett, J.P., Tada, R., 2004. Intermittent existence of a southern Californian upwelling cell during submillennial climate change of the last 60 kyr. Paleoceanography 19, 1–15. https://doi.org/10.1029/2003PA000965

Hernes, P.J., Benner, R., 2002. Transport and diagenesis of dissolved and particulate terrigenous organic matter in the North Pacific Ocean. Deep. Res. Part I Oceanogr. Res. Pap. 49, 2119–2132. https://doi.org/10.1016/S0967-0637(02)00128-0

Hinga, K.R., Arthur, M.A., Pilson, M.E.Q., Whitaker, D., 1994. Carbon isotope fractionation by marine phytoplankton in culture: The effects of CO_2 concentration, pH, temperature, and

species. Global Biogeochem. Cycles 8, 91–102. https://doi.org/10.1029/93GB03393

Jia, G., Li, Z., 2011. Easterly denitrification signal and nitrogen fixation feedback documented in the western Pacific sediments. Geophys. Res. Lett. 38, 1–4. https://doi.org/10.1029/2011GL050021

Kao, S.J., Liu, K.K., Hsu, S.C., Chang, Y.P., Dai, M.H., 2008. North Pacific-wide spreading of isotopically heavy nitrogen during the last deglaciation: Evidence from the western Pacific. Biogeosciences 5, 1641–1650. https://doi.org/10.5194/bg-5-1641-2008

Keeling, C.D., Brix, H., Gruber, N., 2004. Seasonal and long-term dynamics of the upper ocean carbon cycle at Station ALOHA near Hawaii. Global Biogeochem. Cycles 18, 1–26. https://doi.org/10.1029/2004GB002227

Kienast, M., 2000. Unchanged nitrogen isotopic composition of organic matter in the South China Sea during the last climatic cycle: Global implications. Paleoceanography 15, 244–253. https://doi.org/10.1029/1999PA000407

Kienast, M., Lehmann, M.F., Timmermann, A., Galbraith, E., Bolliet, T., Holbourn, A., Normandeau, C., Laj, C., 2008. A mid-Holocene transition in the nitrogen dynamics of the western equatorial Pacific: Evidence of a deepening thermocline? Geophys. Res. Lett. 35, 1–5. https://doi.org/10.1029/2008GL035464

Kienast, S.S., Calvert, S.E., Pedersen, T.F., 2002. Nitrogen isotope and productivity variations along the northeast Pacific margin over the last 120 kyr: Surface and subsurface paleoceanography. Paleoceanography 17, 7-1-7–17. https://doi.org/10.1029/2001PA000650

Langton, S.J., Linsley, B.K., Robinson, R.S., Rosenthal, Y., Oppo, D.W., Eglinton, T.I., Howe, S.S., Djajadihardja, Y.S., Syamsudin, F., 2008. 3500 yr record of centennial-scale climate variability from the Western Pacific Warm Pool. Geology 36, 795–798.

https://doi.org/10.1130/G24926A.1

Locarini, R.A., Mishonov, A. V., Antonov, J.I., Boyer, T.P., Garcia, H.E., Baranova, O.K., Zweng, M.M., Johnson, D.R., 2010. World Ocean Atlas 2009, Volume 1: Temperature., World. https://doi.org/10.1182/blood-2011-06-357442

McKay, J.L., Pedersen, T.F., Kienast, S.S., 2004. Organic carbon accumulation over the last 16 kyr off Vancouver Island, Canada: Evidence for increased marine productivity during the deglacial. Quat. Sci. Rev. 23, 261–281. https://doi.org/10.1016/j.quascirev.2003.07.004

Pichevin, L.E., Ganeshram, R.S., Francavilla, S., Arellano-Torres, E., Pedersen, T.F., Beaufort, L., 2010. Interhemispheric leakage of isotopically heavy nitrate in the eastern tropical Pacific during the last glacial period. Paleoceanography 25, 1–15. https://doi.org/10.1029/2009PA001754

Pichevin, L.E., Reynolds, B.C., Ganeshram, R.S., Cacho, I., Pena, L., Keefe, K., Ellam, R.M., 2009. Enhanced carbon pump inferred from relaxation of nutrient limitation in the glacial ocean. Nature 459, 1114–1117. https://doi.org/10.1038/nature08101

Quay, P., Sonnerup, R., Westby, T., Stutsman, J., McNichol, A., 2003. Changes in the $^{13}C/^{12}C$ of dissolved inorganic carbon in the ocean as a tracer of anthropogenic CO_2 uptake. Global Biogeochem. Cycles 17, 1004, 1-20. https://doi.org/10.1029/2001GB001817

Rafter, P.A., Charles, C.D., 2012. Pleistocene equatorial Pacific dynamics inferred from the zonal asymmetry in sedimentary nitrogen isotopes. Paleoceanography 27, 1–8. https://doi.org/10.1029/2012PA002367

Rau, G.H., Riebesell, U., Wolf-Gladrow, D., 1996. A model of photosynthetic ^{13}C fractionation by marine phytoplankton based on diffusive molecular CO_2 uptake. Mar. Ecol. Prog. Ser. 133, 275–285. https://doi.org/10.3354/meps133275

Rau, G.H., Takahashi, T., Des Marais, D.J., 1989. Latitudinal variations in plankton $\delta^{13}C$: implications for CO_2 and productivity in past oceans. Nature 341, 516–518. https://doi.org/10.1038/341516a0

Rau, G.H., Takahashi, T., Desmarais, D.J., Repeta, D.J., Martin, J.H., 1992. The relationship between $\delta^{13}C$ of organic matter and [CO_2 (aq)] in ocean surface water: Data from a JGOFS site in the northeast Atlantic Ocean and a model. Geochim. Cosmochim. Acta 56, 1413–1419. https://doi.org/10.1016/0016-7037(92)90073-R

Reimer, P.J., Brown, T. a, Reimer, R.W., 2004. Discussion: Reporting and Calibration of Post-Bomb 14C Data. Radiocarbon 46, 1299–1304. https://doi.org/10.2458/azu_js_rc.46.4183

Reimer, P.J., Bard, E., Bayliss, A., Beck, J.W., Blackwell, P.G., Ramsey, C.B., Buck, C.E., Cheng, H., Edwards, R.L., Friedrich, M., Grootes, P.M., Guilderson, T.P., Haflidason, H., Hajdas, I., Hatté, C., Heaton, T.J., Hoffmann, D.L., Hogg, A.G., Hughen, K.A., Kaiser, K.F., Kromer, B., Manning, S.W., Niu, M., Reimer, R.W., Richards, D.A., Scott, E.M., Southon, J.R., Staff, R.A., Turney, C.S.M., van der Plicht, J., 2013. IntCal13 and Marine13 Radiocarbon Age Calibration Curves 0–50,000 Years cal BP. Radiocarbon 55, 1869–1887. https://doi.org/10.2458/azu_js_rc.55.16947

Roark, E.B., Guilderson, T.P., Dunbar, R.B., Fallon, S.J., Mucciarone, D.A., 2009. Extreme longevity in proteinaceous deep-sea corals. Proc. Natl. Acad. Sci. U. S. A. 106, 5204–8. https://doi.org/10.1073/pnas.0810875106

Robinson, R.S., Martinez, P., Pena, L.D., Cacho, I., 2009. Nitrogen isotopic evidence for deglacial changes in nutrient supply in the eastern equatorial Pacific. Paleoceanography 24, PA4213, 1-12. https://doi.org/10.1029/2008PA001702

Stuiver, M., Polach, H.A., 1977. Discussion Reporting of ^{14}C Data. Radiocarbon 19, 355–363.

https://doi.org/10.1017/S0033822200003672

Stuiver, M., Reimer, P.J., and Reimer, R.W., 2017, CALIB 7.0.2 Program available at http://calib.org, accessed 2017.

Takahashi, T., Sutherland, S.C., Wanninkhof, R., Sweeney, C., Feely, R.A., Chipman, D.W., Hales, B., Friederich, G., Chavez, F., Sabine, C., Watson, A., Bakker, D.C.E., Schuster, U., Metzl, N., Yoshikawa-Inoue, H., Ishii, M., Midorikawa, T., Nojiri, Y., Körtzinger, A., Steinhoff, T., Hoppema, M., Olafsson, J., Arnarson, T.S., Tilbrook, B., Johannessen, T., Olsen, A., Bellerby, R., Wong, C.S., Delille, B., Bates, N.R., de Baar, H.J.W., 2009. Climatological mean and decadal change in surface ocean pCO_2, and net sea-air CO_2 flux over the global oceans. Deep. Res. Part II Top. Stud. Oceanogr. 56, 8-10, 554-577. https://doi.org/10.1016/j.dsr2.2008.12.009

Tesdal, J.E., Galbraith, E.D., Kienast, M., 2013. Nitrogen isotopes in bulk marine sediment: Linking seafloor observations with subseafloor records. Biogeosciences 10, 101–118. https://doi.org/10.5194/bg-10-101-2013

Thunell, R.C., Kepple, A.B., 2004. Glacial-Holocene δ15N record from the Gulf of Tehuantepec, Mexico: Implications for denitrification in the eastern equatorial Pacific and changes in atmospheric N_2O. Global Biogeochem. Cycles 18, 1–12. https://doi.org/10.1029/2002GB002028

Vogel, J.S., Nelson, D.E., Southon, J.R., 1987. ^{14}C background levels in an accelerator mass spectrometry system. Radiocarbon 29, 323–333. https://doi.org/10.1017/S0033822200043733

Young, J.N., Bruggeman, J., Rickaby, R.E.M., Erez, J., Conte, M., 2013. Evidence for changes in carbon isotopic fractionation by phytoplankton between 1960 and 2010. Global

Biogeochem. Cycles 27, 505–515. https://doi.org/10.1002/gbc.20045